LANGMUIR

pubs.acs.org/Langmuir Article

# Motile Bacteria at Oil−Water Interfaces: *Pseudomonas aeruginosa*

Jiayi Deng,[†] Mehdi Molaei,[†] Nicholas G. Chisholm, and Kathleen J. Stebe*

Cite This: https://dx.doi.org/10.1021/acs.langmuir.9b03578 Read Online

ACCESS | Metrics & More | Article Recommendations | Supporting Information

**ABSTRACT:** Bacteria are important examples of active or self-propelled colloids. Because of their directed motion, they accumulate near interfaces. There, they can become trapped and swim adjacent to the interface via hydrodynamic interactions, or they can adsorb directly and swim in an adhered state with complex trajectories that differ from those in bulk in both form and spatiotemporal implications. We have adopted the monotrichous bacterium *Pseudomonas aeruginosa* PA01 as a model species and have studied its motion at oil−aqueous interfaces. We have identified conditions in which bacteria swim persistently without restructuring the interface, allowing detailed and prolonged study of their motion. In addition to characterizing the ensemble behavior of the bacteria, we have observed a gallery of distinct trajectories of individual swimmers on and near fluid interfaces. We attribute these diverse swimming behaviors to differing trapped states for the bacteria in the fluid interface. These trajectory types include Brownian diffusive paths for passive adsorbed bacteria, curvilinear trajectories including curly paths with radii of curvature larger than the cell body length, and rapid pirouette motions with radii of curvature comparable to the cell body length. Finally, we see interfacial visitors that come and go from the interfacial plane. We characterize these individual swimmer motions. This work may impact nutrient cycles for bacteria on or near interfaces in nature. This work will also have implications in microrobotics, as active colloids in general and bacteria in particular are used to carry cargo in this burgeoning field. Finally, these results have implications in engineering of active surfaces that exploit interfacially trapped self-propelled colloids.

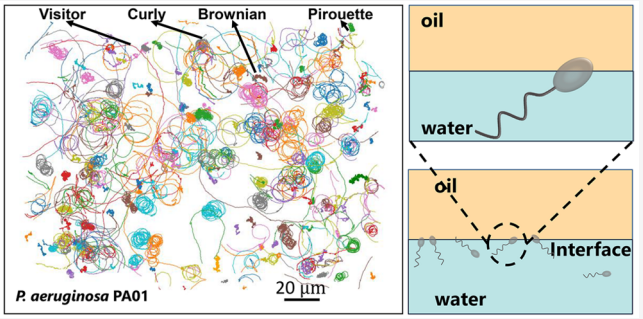




## INTRODUCTION

Understanding the motion of bacteria has clear implications in biology; motile bacteria play important roles in bacteria translocation, and their interactions with boundaries have broad implications in their ability to seed new communities and to form protective biofilms. Bacteria are also excellent examples of self-propelled or active colloids. Too small to be influenced by gravitational forces, these microbes consume fuel to swim. Other examples of active colloids include broad ranges of catalytically driven colloids including Janus beads, multicomponent nanorods,[1] and enzymatically driven colloids.[2] Bacteria can also attach to objects and shuttle them about as cargo.[3] This phenomenon is of recent interest in microrobotics,[4−10] where bacteria laden with cargo are studied as functional microbiohybrids. The swimmers themselves, or their cargo, can be functional structures or loaded with molecules for release. Studies of transport phenomena of bacteria suspensions inform such applications. While near-field effects alter details of motion, all active colloids obey similar hydrodynamic descriptions in the far field, and so studies of swimming bacteria have broad and general significance for all active colloids. To motivate our work, we briefly review relevant literature.

**Structure of *Pseudomonas aeruginosa* and Its Swimming Behavior.** We study *Pseudomonas aeruginosa* PA01 trapped near or on the planar interfaces of aqueous suspension and hexadecane. We have found that when the aqueous phase contains Tris buffer, these bacteria can swim for hours without significantly restructuring the interface, allowing detailed and prolonged observation of their motion. *P. aeruginosa* PA01 are monotrichous bacteria, propelled by a single flagellum. These bacteria have weakly elongated cell bodies of ∼1 μm long with a single flagellum being 5−10 μm in length. The single flagellum of *P. aeruginosa* is located at the pole at one end of the cell body.[11] In general, the bacterial flagellum consists of a cell-envelope-embedded motor, a hook, and a helical filament. These parts work as a reversible rotary motor, a universal joint, and a propeller, respectively.[12] Flagellar motion is powered by an ion flux. The hook connecting the flagellum and cell body is an elastic protein, whose bending stiffness is ∼0.2 pN.[13,14] The morphological details of *P. aeruginosa* are also known; the left handed helical filament has a diameter of ∼20 nm and an amplitude of ∼0.5

Special Issue: Advances in Active Materials

Received: November 18, 2019
Revised: January 27, 2020
Published: February 25, 2020

$\mu$m. The poles of their bodies are decorated with type IV pili, retractable, flexible filaments that are ~1 $\mu$m long and ~5.2 nm in diameter.[15,16] *P. aeruginosa* are Gram-negative bacteria with two cell envelope membranes whose functions are also well characterized. Certain aspects of their colloidal interactions are also understood. For example, the zeta potential of the cell is ~9 mV in saline.[17]

An important feature of *P. aeruginosa* bacteria is their ability to switch between "pusher" or "puller" modes of swimming, which result in extensile or contractile flow along the axis of swimming, respectively. In either mode, they are efficient swimmers, moving at velocities in excess of 10 body lengths per second at Reynolds numbers $Re \sim 1 \times 10^{-4}$. Here, $Re \equiv Ua/\nu$, where $U \sim 10$ $\mu$m/s is the characteristic velocity of the bacterium, $a \sim 1$ $\mu$m is its characteristic length, and $\nu \approx 1 \times 10^{-6}$ $\mu m^2/s$ is the characteristic kinematic viscosity of water. Since $Re \ll 1$, inertia can be neglected when considering their motion. In pusher mode, the flagellum rotates in the counterclockwise (CCW) direction, generating thrust to propel the bacterium forward. The thrust is counterbalanced by viscous drag on the cell body. Furthermore, the cell body rotates in the opposite sense of the flagellum to balance hydrodynamic torque. This is the pusher mode, with leading order hydrodynamic multipole being a force dipole or stresslet. This function determines the form of the velocity field in the far field. Pushers have flow directed away from the bacterium along its direction of motion and toward the bacterium along its sides, whereas in the puller mode the sense of flagellar rotation is reversed. Fluid is instead drawn toward the bacterium, reversing the translation direction and generating a stresslet with opposite sign. In bulk, *P. aeruginosa* change from pusher to puller mode with random, symmetric distributions of transit times (durations of pusher and puller mode subtrajectories). Speeds are also symmetric, reflecting the unbiased regulation of the flagellar motor.[18,19] There is a signature pause when changing between pusher and puller modes that allows switching events to be clearly identified. Monotrichous bacteria flagella can also bend and flick, increasing the complexity of cell motions.[20−22]

**Bacteria as Model Active Colloids.** The reader is referred to recent review articles on active colloids for a more global discussion.[1,23] Broadly, the field of active colloids has grown from two communities. One body of work focused on studies of individual swimmers to understand the implications of hydrodynamics in biology; see, for example, refs 24 and 25. Another body of research was spurred by seminal work[26] in which interactions of bacteria and passive colloids in suspension were studied. The random motion of tracers was reminiscent of thermal motion, but not subject to the equipartition theorem fundamental to statistical behavior of equilibrium systems.

There has since been explosive interest in this domain, including the hydrodynamics of individual swimmers,[27−33] their collective behaviors, and their ability to form structures.[25,34−46] In bulk fluids, ensembles of bacteria interact with each other,[47] or with passive colloids,[26] to form colloidal suspensions with enhanced effective diffusivities determined in part by their active propulsion and in part by thermal interactions. The active part of this effective diffusive motion relies on the swimmers moving along trajectories with random directional reorientation events. After many such events, the active colloid motion resembles a random walk, with mean-squared displacements (MSD) with effective diffusivities that are orders of magnitude greater than those from thermal motion. New phenomena have been revealed including nonequilibrium phase separations,[48−51] negative suspension viscosities,[52] and rheotaxis, in which active colloids swim against[53,54] or normal[55,56] to prevailing flows. Effective transport in active suspensions has been characterized, including the aforementioned effective diffusivities or collective motion,[57,58] to name but a few of the important avenues of research.

Because of their polarized motion, active colloids, including bacteria, accumulate near boundaries.[59,60] Bacteria can also interact hydrodynamically and sterically with solid boundaries and swim adjacent to them in persistent motions.[61−64] Furthermore, bacteria can adsorb onto boundaries. On solid surfaces, such adsorption prevents their translation. In spite of this constraint, adsorption provides interesting opportunities for solid surface engineering. Direct adhesion of bacteria to solid surfaces, for example, by flagella or pili, has been reported, resulting in bacteria that rotate around a fixed point tracing paths with curvatures and form related to their adhered state.[18,65−67] Bacteria can also form structures influenced by adhesion; for example, in an adhered state, the polar flagellar filament can execute a polymorphic change into a spiral-like state that wraps around the cell body.[68] Flagellated bacteria adhered to solid surfaces have been studied as active carpets that promote mixing.[69−71] In simulation, such active carpets are predicted to generate spatiotemporal patterns with significant coherent flows and associated nutrient fluxes toward the surface.[69] Adsorption at fluid interfaces also presents interesting possibilities. Fluid interfaces are mobile, so adsorption does not prevent translation. Adsorbed bacteria can swim along the interface, an important degree of freedom. However, adsorption to a fluid interface does constrain bacteria motion in important ways. These constraints give rise to different swimming modalities that we explore in this paper. Bacteria can also restructure boundaries by forming biofilms on solid surfaces[72−81] or films of bacteria at fluid interfaces,[82−84] a phenomenon we have studied in prior research. We do not consider such restructuring here, as we have identified settings in which this does not occur, allowing us to focus on motile bacteria.

**Bacteria Swimming near Solid Boundaries.** Bacteria swimming adjacent to solid boundaries have been extensively studied. Bacteria interact with boundaries via hydrodynamic[27,59,85,86] and steric interactions.[30,61−63,87,88] Pullers accumulate near solid surfaces because of their polarized motion,[59−61,89] with stable orientation perpendicular to the surface.[27] Their fate depends on the angle with respect to the surface and the orientation of their cell body.[27,61,90] Pullers with cell bodies oriented away from the surface can pull themselves onto the surface, promoting adhesion, while pullers with cell bodies oriented toward the surface can be pulled away. Pushers swim and accumulate adjacent to solid surfaces and remain in planes adjacent to the surface,[30,59,85−87,91] a phenomenon referred to as trapping. Such trapping near solid surfaces has been attributed to steric[87] and hydrodynamic interactions.[59] Hydrodynamic interactions also cause pushers to reorient parallel to the surface[59,85,86] in persistent circular swimming paths.[91−94] These curvilinear paths can be understood in terms of the drag asymmetry introduced by the solid boundary. Surfaces of the flagellum and cell body closer to the solid boundary experience greater drag. Since the flagellum and body rotate in opposite directions, they generate a force couple


https://dx.doi.org/10.1021/acs.langmuir.9b03578
Langmuir XXXX, XXX, XXX−XXX

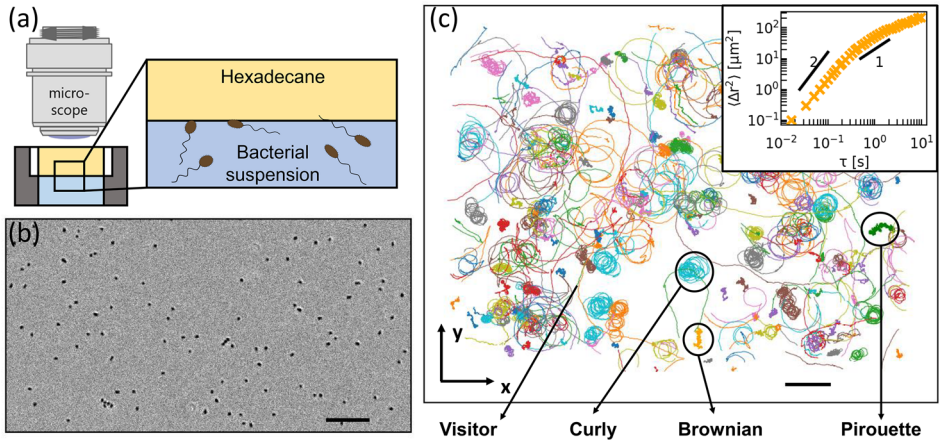


**Figure 1.** Schematic of the experiment and ensemble behavior of *Pseudomonas aeruginosa* PA01. (a) Schematic of the experimental setup. (b) Top view of the interface between bacterial suspension and hexadecane. Half of the field of view is shown. Black ellipsoids represent the bacteria. (c) Individual bacteria trajectories are shown only over a 20 s time span for clarity. Four distinct trajectory types are identified. Active motions include (i) interfacial visitors and two types of persistent circular motions including (ii) pirouettes and (iii) curly trajectories. A fourth trajectory type (iv), inert Brownian diffusive bacteria, is also present. Scale bar is 20 $\mu$m. Inset: ensemble mean-squared displacement (eMSD) of all bacteria.

or opposing lateral forces on the flagellum and cell body. This generates a torque that rotates the bacterium clockwise (CW), resulting in circular paths in planes parallel to the boundary. Hydrodynamic interactions with the boundary increase swimming speed parallel to the surface[91,95] and retard velocities perpendicular to the surface.[62]

Bacteria are also subject to thermal Brownian motion which is coupled to active swimming. For example, diffusive changes in the bacteria's orientation and distance from the boundary can significantly alter the swimming speed and radius of curvature of the swimming trajectory.[88] From far-field hydrodynamic considerations, pushers are expected to be attracted toward boundaries and align parallel to them and pullers are predicted to align perpendicular to the boundary and thus either dive toward it or escape. Near solids, pushers are expected to swim in CW circles and pullers in CCW circles. However, near-field and physicochemical interactions with solids can change this scenario, as revealed in a study comparing pushers to pullers.[89] For example, monotrichous bacteria near solid surfaces have an asymmetric swimming pattern, with straighter paths during "runs" and more curved paths in "reverse". Moreover, on average, near boundaries, backward swimming is faster than forward swimming.[88,89,96−98] Furthermore, while hydrodynamic interactions are predicted to trap pushers, a pusher bacterium (*Vibrio alginolyticus* NMB136) was able to escape from solid surfaces more effectively than a puller bacterium (*Vibrio alginolyticus* NMB102).[89] In this study, the pushers changed their inclination angle with respect to the solid surface and moved away, whereas the pullers "backed up" and collided with the solid surface, becoming trapped by adsorption of their flagellum.

Changes in swimmer motion near boundaries also modify transport and effective diffusion processes, which depend on trajectory velocity, reorientation time scales, and thermal diffusion,[99,100] all of which are altered by boundaries. Analyses of MSD of swimmers near solid boundaries with particular persistent trajectory types, for example, runs and reversals,[101,102] indeed demonstrate strong dependence of effective diffusion processes on the details of the trajectories. Hydrodynamic analyses also predict enhanced tracer diffusion with respect to the bulk at intermediate distances from a solid wall due to the symmetry-breaking influence of hydrodynamic images.[103] Finally, bacteria near solid surfaces can form elaborate self-organized structures. For example, surface associated, perpendicularly aligned *Thiovulum majus* generates a "tornado-like" flow and interacts hydrodynamically with neighboring bacteria to form an assembly of bacteria with crystalline order.[104,105] An analysis of this perpendicular alignment reveals that this surface bound state is stable only for bacteria possessing flagella shorter than a critical length.[106] Many of these interactions are not limited to bacteria and have been observed for chemically driven artificial Janus swimmers as well. For example, hydrodynamic interactions contribute to guided motion of self-diffusiophoretic colloidal probes along the no-slip boundaries.[107,108]

**Bacteria Swimming near Fluid Interfaces.** The literature for bacteria swimming near fluid interfaces is less developed. Adjacent to fluid interfaces, bacteria also swim in circular paths. CCW circular paths have been observed for pushers near free surfaces or air−aqueous interface,[109] with their cell body tilted toward the interface.[110] Drag asymmetry arguments like those for bacteria near solid boundaries, amended to note the weak dissipation in the air phase, may explain the bacteria's circular, CCW paths at free surfaces. Surfactants or adsorbed proteins alter interface mobility and change this sense of rotation. For example, both CW and CCW motions occur for pushers at heterogeneous free surfaces[111] partially covered with surfactant, and a reversal from CCW to CW rotation occurs on interfaces with adsorbed protein layers.[112] Synthetic catalytic swimmers[113−115] also follow complex paths at interfaces, with enhanced motion being attributed to the adhesion state biasing the propulsion mechanism. Circular motions, promoted either by the shape of the Janus caps or of the swimmers themselves, have also been reported at interfaces.[116,117] Multiflagellated bacteria have been reported to adsorb at interfaces in near vertical alignments to generate 3D flow fields with radially directed flow in the interface adjacent to the swimmer that promotes cluster formation.[118] In prior work, we reported curvilinear paths with different radii of curvature for colloids at interfaces carried as cargo by adhered bacteria[3] and for the bacteria themselves


https://dx.doi.org/10.1021/acs.langmuir.9b03578
Langmuir XXXX, XXX, XXX−XXX

adhered to the interface. These motions are attributed to modes associated with nonuniform propulsion mechanisms, colloid shape, or adhesion state. Such nonuniform propulsion mechanisms are known to generate helical trajectories in bulk.[5,8,119−122] Ensembles of active Janus beads have also been studied at fluid interfaces to explore concepts of swim pressure; particle distributions were studied in acoustic traps adjacent to fluid interfaces and obey predicted population dynamics.[45]

In this study, we study the trajectories of bacteria at the interface of hexadecane with an aqueous suspension of bacteria at relatively dilute bacterial surface concentrations. We observe several distinct swimming modes and characterize these modes in terms of the statistical properties of their trajectories. We hypothesize that different categories of trajectories correspond to different adsorbed states of the bacteria and discuss inferred adsorbed configurations. We also report behaviors at free surfaces and at silicone oil interfaces of varying viscosity.

## EXPERIMENTAL SECTION

**Bacteria Suspension Preparation.** *P. aeruginosa* PA01 wild type and ΔpilC are inoculated and cultured in 10 mL of lysogeny broth (LB) using a 50 mL conical flask with a porous cap. The cultures are placed on a tabletop shaker at 250 rpm at 37.0 °C for 17 h. They were then centrifuged at 3500 rpm for 10 min. After centrifugation, the sediment is washed and resuspended with Tris-based motility medium (50 mM Tris-HCl, pH = 7.5, 5 mM $MgCl_2$, 5 mM glucose, 200 mM NaCl, and 100 mM KCl). This centrifugation and resuspension process is repeated twice to prepare a bacteria suspension. The cell concentration is determined by optical density measurements at 630 nm using an Infinite 200 PRO instrument. The optical density for our experiments was set to be 0.05. A cylindrical vessel with an inner diameter of 1 cm is covered with a glass coverslip at the bottom and sealed with vacuum grease (Figure 1a). The bottom half of the cylinder is aluminum, and the top half is Teflon. These two parts intersect in the middle and pin the interface, thus creating a planar oil−water interface. The aqueous bacteria suspension of approximately 115 μL is placed in the bottom of the vessel, and 500 μL of hexadecane is then pipeted into the vessel to form an oil−water interface. We also varied the viscosity of the nonaqueous phase, using air to give a nearly vanishing viscosity ratio and different silicone oils to yield viscosity ratios between 1 and 300. Experimental methods remain the same for silicone oil experiments.

**Imaging.** The bacteria motion is imaged using an upright microscope (Zeiss AxioImager M1m) in bright field with 50×magnification. The videos are recorded by a high-speed camera at 61 frames per second. We calculate the background noise by averaging over all frames in the video and subtract that noise from the original images (Figure 1b). Bacteria on the interface appear as ellipsoidal dark regions with an area of approximately 2 $\mu m^2$, while bacteria adjacent to the interface appear white as they are out of the interfacial plane. Bacteria that remain dark in color throughout the observation time (up to 1 min) are inferred to be adhered to the interface. We define the oil−water interface as the $x$−$y$ plane, where the $x$-axis is the horizontal direction of the image. The coordinate $z$ is defined downward into the fluid.

**Cell Tracking and Analysis.** To extract information about the cell body, the microscopic images are further processed using Otsu thresholding to locate the features and are analyzed using the open software Python regionprops function to extract properties of their ellipsoidal shape. The input images are transformed into an $(N, M)$ array with the featured pixels labeled as value 1 and the rest labeled as value 0. The aspect ratio of this ellipse $\gamma$ is calculated as the length (in pixels) of the major axis of the ellipse divided by the length (in pixels) of the minor axis of the ellipse.

Bacteria trajectories are extracted using a custom Python implementation of the Crocker−Grier multiple-particle tracking algorithm.[123] Here, we defined the cell body axis as the major axis of the ellipse. We find the centroid of the ellipse around the cell body. We follow the trajectory of the centroid to define the path or trajectory of the individual swimmer. A sample of trajectories is shown in Figure 1c for the time span of 20 s. We focus on extracting information from individual trajectories over time $t$ and, where relevant, lag time $\tau$.

The instantaneous orientation of bacteria, $\phi \in (-\pi/2, \pi/2]$, is defined as the angle between the body axis and $x$-axis of the interface; the range of $\phi$ in calculation of the orientation is limited because the body axis is a headless vector. From this angle, the instantaneous rotational angular velocity is calculated as $\Omega = (\phi(t + \Delta t) - \phi(t))/\Delta t$. For some trajectories, the rotational autocorrelation function, $A_R(\tau) = \langle \Omega(t + \tau)\, \Omega(t)\rangle_t / \langle \Omega^2(t)\rangle_t$, is used to characterize rotational motion in the interface, where $\Omega$ is assumed to be stationary. The swimming direction is also extracted for each time step and used to calculate the directional autocorrelation function at a given lag time; $A_D(\tau) = \langle \boldsymbol{n}(t + \tau)\cdot\boldsymbol{n}(t)\rangle_t$, where $\boldsymbol{n} = (n_x, n_y)$ is the unit vector in the direction of the swimming velocity between two frames. To calculate path curvature at each time step, the trajectories are smoothed using a third-order Savitztky−Golay filter with a window size of 25 frames. The swimming direction, $\phi_s \in (-\pi, \pi]$, is defined as the angle between bacterial velocity vector and the fixed $x$-axis. The swimming speed is calculated as a function of time for individual trajectories according to $v = |\boldsymbol{r}(t + \Delta t) - \boldsymbol{r}(t)|/\Delta t$, where the position vector at each frame is $\boldsymbol{r}(t) = (x(t), y(t))$. The trajectory curvature is calculated as $\kappa = -[\boldsymbol{r}'(t) \times \boldsymbol{r}''(t)]\cdot\boldsymbol{e}_z/|\boldsymbol{r}'(t)|^3$, where primes indicate derivatives with respect to time $t$ and $\boldsymbol{e}_z$ is the unit vector in the $z$ direction. The center of curvature of the curvilinear path $(x_c, y_c)$ is calculated based on the curvature $\kappa$ and swimming direction at each frame, with $x_c = x - n_y/\kappa$ and $y_c = y + n_x/\kappa$.

Switching events between pusher and puller modes are distinguished using two criteria, a concomitant rapid change of trajectory curvature and a low instantaneous speed (<5 μm/s). Each single trajectory is divided into clockwise (CW) and counterclockwise (CCW) segments according to the median curvature of each segment. Throughout this study, the rotational sense, that is, CCW or CW, is defined with respect to the fluid interface when viewed from the water side. The mean-squared displacement (MSD), defined as the average of the squared displacements at lag time $\tau$ over the course of the trajectory $\langle \Delta \boldsymbol{r}^2(\tau)\rangle = \langle (\boldsymbol{r}(t + \tau) - \boldsymbol{r}(t))^2\rangle_t$, is calculated to characterize the translational motion of the bacteria. The mean-squared angular displacements (MSAD), defined as $\langle \Delta\phi^2(\tau)\rangle = \langle (\phi(t + \tau) - \phi(t))^2\rangle_t$, is also calculated to characterize the rotational motion of the bacteria. To eliminate the discontinuities in angles near $\pm\pi/2$, we calculate the bounded MSAD using the absolute value of orientation angle. Thus, $\phi$ is limited to $(0, \pi/2)$, and the bounded MSAD follows a stretched exponential function[124]

$$\langle \Delta\phi^2(\tau)\rangle_b = \langle \Delta\phi^2(\infty)\rangle_b \left\{ 1 - \left( 1 - \frac{2\varepsilon_\phi{}^2}{\langle \Delta\phi^2(\infty)\rangle_b} \right) \times \exp[-\xi(2D_R\tau)^\varsigma] \right\} \quad (1)$$

where $\xi = 0.968$ and $\varsigma = 0.962$ are stretched exponential parameters (see Supporting Information SI1) and $\varepsilon_\phi$ is the static noise in the orientation. The asymptotic value of the bounded MSAD can be determined based on the probability distribution of $\phi$. Since, after randomly diffusing for a long time, $\phi$ is uniformly distributed between 0 and $\pi/2$ and $P(\phi; t \to \infty) = 2/\pi$; thus,

$$\langle \Delta\phi^2(\infty)\rangle_b = \frac{4}{\pi^2} \int_0^{\pi/2} d\phi_2 \int_0^{\pi/2} (\phi_1 - \phi_2)^2\, d\phi_1 = \frac{\pi^2}{24} \quad (2)$$

## RESULTS AND DISCUSSION

Results for PA01 are presented at Tris buffer suspension−hexadecane interfaces for dilute systems, with 0.005 bacteria/$\mu m^2$, corresponding to a fractional surface coverage of 0.0075.


https://dx.doi.org/10.1021/acs.langmuir.9b03578
Langmuir XXXX, XXX, XXX−XXX

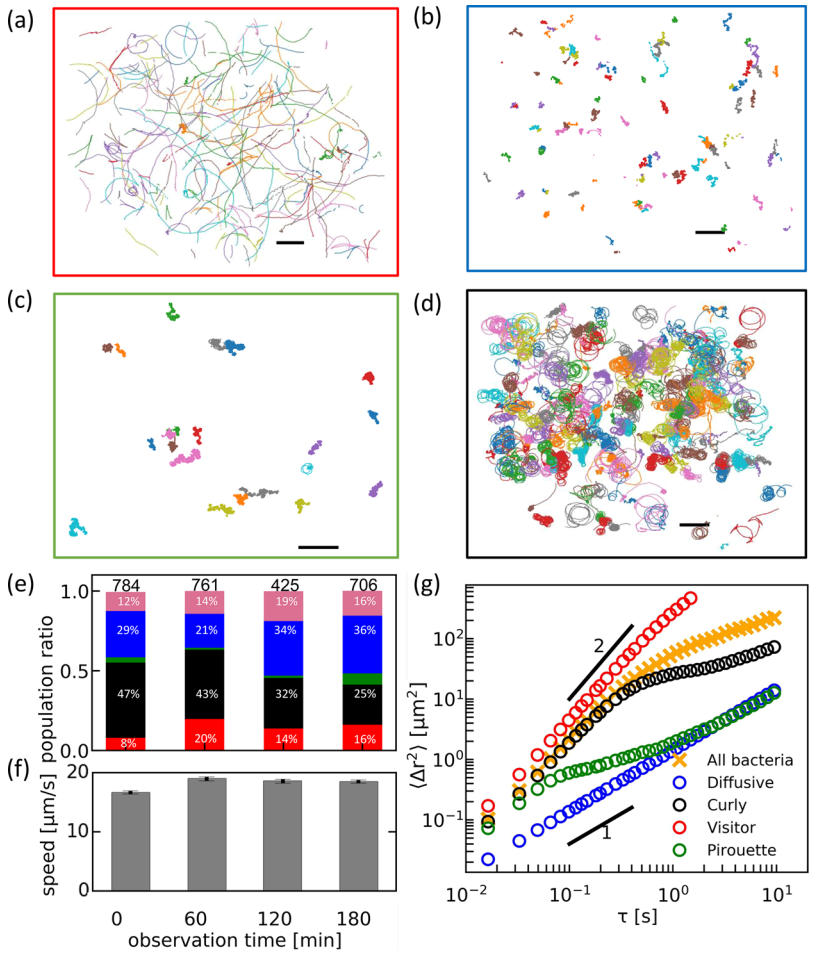


**Figure 2.** Four distinct behaviors are observed on or adjacent to the interface. Individual trajectories are sorted based on their trajectory types and plotted separately with (a) interfacial visitors, (b) Brownian diffusive motion, (c) pirouette motion, and (d) curly motion. Scale bars are 20 $\mu$m. (e) Population ratio of each trajectory type remains roughly fixed after 3 h of observation. Colors for each trajectory types are stated in the legend for (g), except for pink, which represents clustered bacteria. Numbers on top: total number of trajectories. (f) Speed of curly motion remains the same during the observation time. (g) Ensemble mean-squared displacement for each trajectory type. Black lines are guides for the eye for pure diffusive and ballistic motions.

For this system, the ratio of oil to aqueous phase viscosity is $\lambda = \mu_o/\mu_w = 3$. We study this relatively dilute system to capture individual trajectories and reduce the effects of interactions between neighboring bacteria. The ensemble mean-squared displacement (eMSD) of all bacteria, shown in the inset to Figure 1c, shows similar behavior as active swimmers in a 2D film or passive colloids at the interface of an active bath. The ensemble of bacteria moves ballistically for lag times of ~0.4 s. The relatively long time for this ballistic motion indicates the active motion in the interface. The ensemble of bacteria then moves diffusively, as expected after multiple randomizing events in the interface. Furthermore, as expected, the active nature of the system is apparent in effective diffusivities that are far larger than Brownian diffusivities for micrometer scale objects. At the interface, the effective diffusivity for ensembles of bacteria, determined from the diffusive regime of eMSD, is 13.25 $\mu$m$^2$/s, 2 orders of magnitude greater than the diffusivity of a passive colloid with a similar size to the cell body. While the eMSD has important expected signatures, averaging over the ensemble of the swimmers misses important behaviors that are revealed by considering individual trajectories. Such scrutiny reveals four distinct characteristic motions. The ensemble behavior of each trajectory type differs significantly from the behavior obtained by averaging over the entire population; these different forms suggest that these trajectories have differing underlying physics. We delve into the mechanisms for these behaviors below by considering first paths for individual swimmers, identifying essential signatures in the individual paths and ensembles of each trajectory type, and proposing mechanisms.

**Distinct Trajectory Types.** We have observed distinct trajectory types for individual swimmers which we enumerate here. Interfacial visitors do not remain in the plane of the interface (Figure 2a), while we infer that the remaining three types are adsorbed as they remain in the interfacial plane over typical observation times of 60 s. The motions of these adsorbed microbes include bacteria moving by Brownian diffusion (Figure 2b), similar to inert colloids, and two distinct curvilinear swimming behaviors which we term pirouettes (Figure 2c) and curly motions (Figure 2d). The population ratio of each trajectory type (Figure 2e) and the speed of curly motion (Figure 2f) remain roughly unchanged over an observation time of several hours, suggesting stable trapping of the swimming bacteria in distinct configurations. As noted in the Introduction, the Reynolds number characterizing the importance of inertial to viscous momentum transport is


https://dx.doi.org/10.1021/acs.langmuir.9b03578
Langmuir XXXX, XXX, XXX−XXX

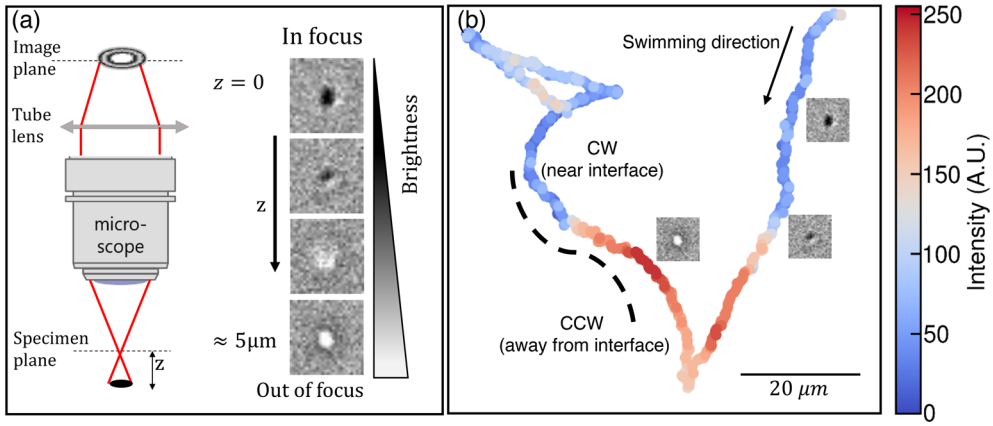


**Figure 3.** Representative trajectory of an interfacial visitor. (a) Schematic of the image formation based on the distance of cells from the specimen plane. Bacteria appear as sharp, dark spots when in focus and as bright, blurry spots when out of focus. Example images of a bacterium with various intensities are shown to illustrate changes in height of approximately 5 $\mu$m. (b) The 2D projection of a typical 3D path of an interfacial visitor, colored by pixel intensity of the bacterial image.

negligible in this system, so viscous effects dominate for swimming bacteria. For bacteria adhered to or swimming adjacent to fluid interfaces, viscous stresses from bacteria motion are far less than stresses related to surface tension that resist interfacial deformation. This comparison is captured by the capillary number $Ca = \mu U/\sigma$, where $\mu$ is the characteristic viscosity of the system and $\sigma$ is the interfacial tension. For our system, $Ca \approx 10^{-5}$, so the viscous stresses generated by swimming bacteria cannot distort the interface.

**Interfacial Visitors.** Interfacial visitors comprise 10−20% of the population of observed swimmer trajectories (Figure 2e). These bacteria are not adhered but swim toward and away from the interface, changing their heights by several micrometers, as evidenced by repeated changes in grayscale from dark to white to dark again over the course of observation (Figure 3a). Therefore, the trajectories measured by optical microscopy are 2D projections of complex 3D paths (Figure 3b). Bacteria that swim adjacent to the interface do not remain in the interfacial plane for prolonged periods of time. For example, we observe the interface for a 60 s time span. Visitors remain adjacent to the interface, as evidenced by the darkness of their cell bodies, for as long as 10 s with a mean duration of 3 s.

The visitor's paths are weakly curvilinear, often switching between CW and CCW. These switches are often associated with changes between pusher and puller propulsion modes and hence coincide with changes in the bacterium's direction of propulsion. Examining many visitor trajectories, we observe that switching events often precede bacterial escape from the interface (Figure S2a), but switching can also occur with no change of distance from the interface (Figure S2b). Furthermore, bacteria can change their distance from the interface without switching modes at all (Figure S2c). We also probed whether time spent at a fixed distance from the interface depends strongly on CW versus CCW swimming; bacteria in both modes are observed to remain adjacent to the interface, (i.e., with black cell bodies) for durations of seconds, as shown in Movie SI_V1 in the Supporting Information and in the trajectory reported in Figure S2b.

Recall that hydrodynamic analysis predicts that pushers should be attracted to boundaries,[59] whereas pullers are expected to crash into walls owing to their polarized motions. In experiment, persistent curvilinear paths are often reported near boundaries, with rotation sense depending on whether the boundary is a solid surface, a free surface, or a surfactant laden interface.[64,92,109,111,112] Furthermore, hydrodynamic analysis predicts that the rotational sense is a function of the swimming mode, fluid properties, and bacterium shape.[125] For a model bacterium swimming near a fluid−fluid interface with viscosity ratio $\lambda$, the hydrodynamically induced rotational velocity is predicted to be[125]

$$\Omega_z^{\text{ind}} = \frac{3}{256\pi}\frac{q}{\mu z^4}\left(\frac{\gamma^{*2}-1}{\gamma^{*2}+1}+\frac{1-\lambda}{1+\lambda}\right) \quad (3)$$

where $q$ is the strength of the rotlet dipole (positive for pushers and negative for pullers) and $\gamma^*$ is the effective total aspect ratio of the cell (including the flagellum). For our system, $\lambda = 3$ and $\gamma^* > \lambda^{1/2}$; thus, the model predicts CCW rotation for pusher mode and CW for puller mode. In this analysis, the predicted sign of the curvature is independent of the distance from the interface. However, our data, which is obtained within body lengths of the interface, show an intriguing depth-dependence on curvature direction. We find that visitors can swim along "S" shaped trajectories as shown in Figure 3b (Movie SI_V2 in the Supporting Information). That is, trajectory curvature changes from CW to CCW curvatures without a corresponding change in swimming direction or switch between swimming modes. Such changes in trajectory curvature near the interface might be related to a transition from far-field-dominated to near-field-dominated hydrodynamic interactions. Equation 3 is based on a far-field "point swimmer" model and thus may not capture near-field effects. These observations should spur future research in the field.

The path and swimming characteristics of visitor trajectories clearly reveal that these bacteria are not adhered to the interface and move with significant speeds over the time of observation. Interfacial visitors move ballistically, along relatively straight paths ($\kappa < 0.1\ \mu m^{-1}$) with maximum speeds in excess of 40 $\mu$m/s and a median swim speed of 27.2 ± 7.21 $\mu$m/s. The absence of a diffusive regime in the eMSD of visitors shown in Figure 2g indicates that randomizing events are insignificant for these swimmers when they are close to the interface.

**Brownian Diffusive Bacteria.** Roughly 30% of the bacteria move with Brownian motion (Figure 2e). Their


https://dx.doi.org/10.1021/acs.langmuir.9b03578
Langmuir XXXX, XXX, XXX−XXX

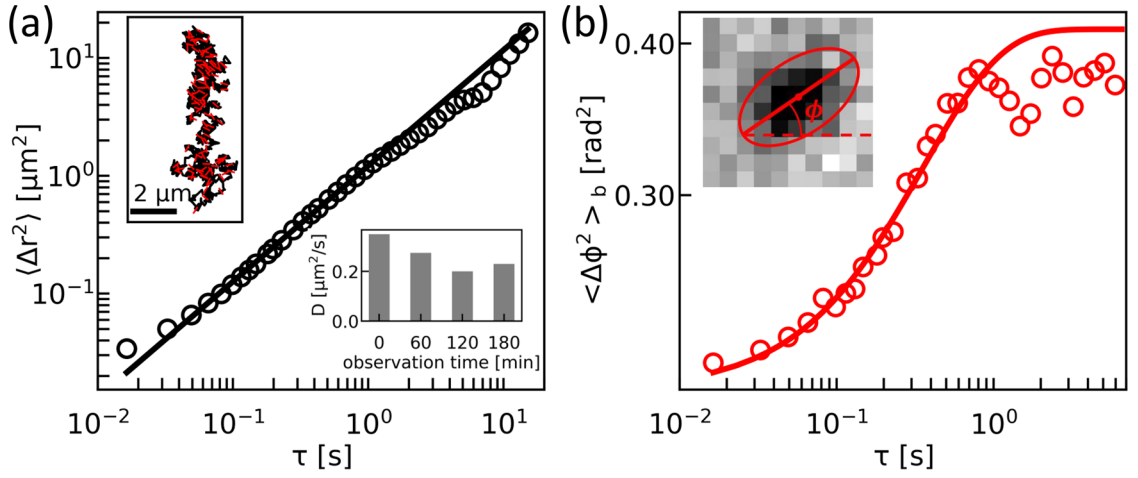


**Figure 4.** Translational and rotational Brownian noise of an individual diffusive bacterium. (a) MSD of the bacterium, circles, with a linear fit, black line. Top inset: trajectory of the bacterium for 30 s. Short red lines indicate the orientation of the bacterium at every 0.25 s. Bottom inset: Diffusion coefficients of eMSD of the diffusive population over 3 h. (b) Bounded MSAD, red circles, with fit to eq 1, red line. Inset: example image of the diffusive bacterium with labeled body orientation.

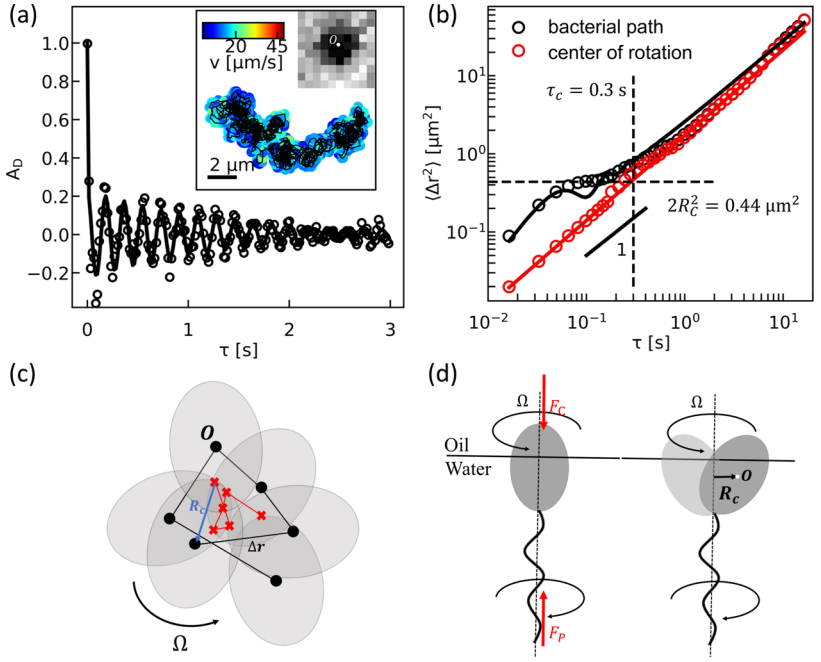


**Figure 5.** Rotational behavior of an individual pirouette bacterium. (a) Directional autocorrelation function $A_D$ calculated from a 6 s segment of the trajectory with oscillation period of $\tau_{osc}$ = 0.18 s with fit to eq 4. Inset: trajectory for 30 s colored by its speed, with the black line revealing the high curvature of its path and an example of its spherical shape image. (b) MSD of the path, black circles, fitted to eq 6, black line, and MSD of the center of the rotation, red circles, with a linear fit, red line. The black dashed lines indicate the subdiffusive plateau $2R_c^2$ and the decorrelation time $\tau_c$ of the "self-caging" behavior. (c) Details of pirouette motion at six selected consecutive frames from the trajectory shown in (a). Location of the centroid: black circles, *and* its trajectory, black line; gray ellipsoids: 2D projection of the cell body and its center of rotation, red crosses. (d) Schematic illustration of the mechanisms of pirouette motion. The cell body is trapped in a weakly tilted state, and the flagellum is aligned normal to the interface. The distance between the axis of flagellum and the centroid of the cell body defines $R_c$.

eMSD is linear in lag time, with thermal diffusivity $D_T$ = 0.35 $\mu$m$^2$/s, similar to an inert 1.5 $\mu$m diameter passive colloid trapped at the hexadecane−water interface. These bacteria are presumably in a sessile, inert state or are trapped in a configuration that denies the molecular motor access to ions that fuel its rotation, for example, by immersion of the motor in the oil phase. A representative trajectory of an individual Brownian diffusive bacterium is studied, inset Figure 4a (Movie SI_V3 in the Supporting Information). Its MSD, as plotted in Figure 4a, yields a thermal diffusivity $D_T$ = 0.3 $\mu$m$^2$/s similar in magnitude to that of the ensemble. The MSAD of this trajectory has form $\langle \Delta\phi^2(\tau) \rangle = 2D_R\tau + 2\varepsilon_\phi^2$, where $D_R$ indicates the rotational diffusivity of the random process and $\varepsilon_\phi$ captures the static noise in the measurement of the angle. Since the measured orientation angle is projected onto a to single arc of a whole circle ($0 \le \phi \le \pi/2$), we fitted the bounded MSAD, $\langle \Delta\phi^2(\tau) \rangle_b$, as given in eq 1 (Figure 4b), to extract the angular diffusion coefficient $D_R$ = 1.21 rad$^2$/s and static noise $\varepsilon_\phi$ = 0.317 rad. This noise indicates that we can measure the orientation to within 20° precision.


https://dx.doi.org/10.1021/acs.langmuir.9b03578
Langmuir XXXX, XXX, XXX−XXX

These data suggest that both the translational and rotational behavior of diffusive bacteria are solely governed by Brownian motion. The diffusive behavior indicates the noise from stochastic thermal fluctuations in the system, which can be used as a baseline to compare with the noise induced by active motion of the swimmers that experience active randomization events. Furthermore, these inert bacteria serve as interfacial probes and confirm that the interface does not restructure to form elastic films over the course of the experiment for time scales of hours. This is indicated by the weak changes in diffusivity of the Brownian diffusive bacteria over the age of the interface (inset to Figure 4a).

**Pirouettes.** Rarely, for approximately 5% of the population, bacteria rotate quickly in nearly fixed positions, like a ballerina on pointe, motivating the term "pirouette" trajectories. For these trajectories, the dark gray spot from the projected cell body in the interface is almost circular rather than elliptical, as shown in the inset to Figure 5a, indicating near vertical alignment of the cell body. We follow the trajectory of the centroid of this spot to define the path. The centroid moves in circular paths with a characteristic radius of curvature smaller than the cell body, as shown in Figure 5a for a representative trajectory. Movie SI_V4 of this trajectory in the Supporting Information shows that pirouetting bacteria rotate quickly and translate slowly; analysis will show that they translate only by Brownian diffusion. We compute the directional autocorrelation function $A_D$ from the direction of the instantaneous velocity along the centroid's path (Figure 5a). The high frequency rotational motion of the bacterium is reflected in the rapid oscillation in this function, from which we measure the oscillation time, $\tau_{osc}$ or equivalently the angular velocity of $\Omega$ = 35 rad/s. From analysis of several paths, we find that pirouettes rotate very rapidly, with angular velocities in the range of $10 \leq \Omega \leq 100$ rad/s. Furthermore, this motion of the centroid is solid body rotation around the center of rotation (Figure 5c). The distance between the centroid and the center of rotation defines the radius of curvature of the path $R_c$. We observe that pirouetting bacteria have path radii of curvature that are very small, smaller than the length of their bodies, <1 $\mu$m with a median value of 0.46 $\mu$m. For this particular trajectory, the curvature is almost fixed in both pusher and puller modes. However, analysis of many pirouettes reveals that some have tighter paths in CCW rotation.

We observe that the center of rotation is moving, as reported in the inset of Figure 5a. The linearity of the MSD of the center of rotation as shown in Figure 5b indicates that this center of rotation moves diffusively, with a diffusivity 0.44 $\mu m^2/s$, similar to the thermal diffusivity. Thus, the pirouetting bacteria have no active translational motion but have active rotational motion with thermal diffusion of the center of rotation.

We also study the MSD of the bacteria's path, shown in Figure 5b. The MSD is initially superdiffusive. Thereafter, a subdiffusive plateau is evident, a signature of "self-caging". These plateau differ from those in MSD of colloidal tracers in, for example, polymeric networks, where the value of the MSD at the plateau indicates the length scale of the physical entrapment of the colloid. Here, the plateau occurs because the bacterium spins in circles, and so explores a domain smaller than would be explored by random displacements. The MSD value for the plateau is defined by the average square distance between two points randomly and uniformly distributed on a circle of radius $R_c$; that is, $2R_c^2 = (\bar{v}\tau_{osc})^2/2\pi^2$, where $\bar{v}$ is the average active rotational velocity and $\tau_{osc}$ = 0.18 s. At long times, diffusion of the center of rotation dominates the active solid body rotation, and the MSD becomes diffusive with the effective diffusion coefficient of $D$ = 0.44 $\mu m^2/s$ similar to the thermal diffusivity and identical to the diffusion of the center of rotation. Therefore, the plateau lifetime is limited by thermal diffusion. The self-caging ends when thermal displacements are similar to the radii of the circular paths, that is, $\sqrt{2D_T\tau_c} \sim R_c$, where the decorrelation time can be estimated as $\tau_c \sim 0.30$ s.

The ensemble MSD of pirouette motion, Figure 2g, shows similar behavior to the MSD of the single trajectory, with the three signature regimes with increasing lag time; superdiffusive, self-caging plateau with the average square distance $2R_c^2 \sim 1$ $\mu m^2$ that decorrelates with a decorrelation time of 1 s. At long lag times, the diffusive regime superposes with the MSD of the Brownian diffusive path, consistent with the translation of pirouettes being determined by thermal fluctuations.

As shown schematically in Figure 5d, we infer a nearly perpendicular alignment of an active bacterium with respect to the interface. The cell body is adhered to the interface, as a bacterium adhered by its flagellum would allow paths with greater radii of curvature. Related configurations and motions have been reported for the multiflagellated bacterium at air–water interfaces.[118] This inferred alignment is consistent with the purely diffusive translational motion and the nearly circular shape (inset to Figure 5a) of the cell body projected into the plane of the interface which has an aspect ratio of approximately $\gamma$ = 1.1. The persistence of the pirouette motion and the roughly circular cross section of the cell body suggest that the contact line where the fluid interface intersects the cell body is pinned preventing changes from this nearly vertical trapped state. A pinned contact line would allow the cell body to rotate about the $z$ axis, but it would preclude rotation around an axis in the $x$–$y$ plane. This suggests that the energetics of contact line pinning are far greater than the torques exerted by the cell body around an axis in the $x$–$y$ plane.

In this limit, we consider a force balance on a bacterium with a cell body and flagellum oriented perpendicular to the interface. In this configuration, the propulsive thrust force $F_P \sim 10^{-13}$ N in the $z$ direction is counterbalanced by the surface tension forces. In the limit of small $Ca$, as applies here, the bacterium does not distort the interface via viscous stresses. Contact line pinning and small $Ca$ also preclude the bacterium from moving in the $z$ direction through the interface. Furthermore, the vertical alignment precludes translation in the $x$–$y$ plane, as there is no thrust in this plane to drive motion. A torque balance is also instructive. The cell body rotates about the $z$ axis. The observed rotational behavior of pirouetting bacteria results from the counter-rotation of cell body to balance the torque created by flagellar rotation. The cell body is trapped in a weakly tilted state, and the flagellum is aligned normal to the interface, as depicted schematically in Figure 5d. The center of rotation coincides with the flagellum axis. The distance between this axis and the centroid of the cell body defines $R_c$.

While these pirouette motions are rare, all observed pirouettes persist over the 60 s observation time. Over these time spans, there is evidence of switching between CW and CCW modes. The stability of vertical spinning of monotrichous bacteria near a solid surface has been analyzed hydrodynamically; elastohydrodynamic coupling between the


https://dx.doi.org/10.1021/acs.langmuir.9b03578
Langmuir XXXX, XXX, XXX–XXX

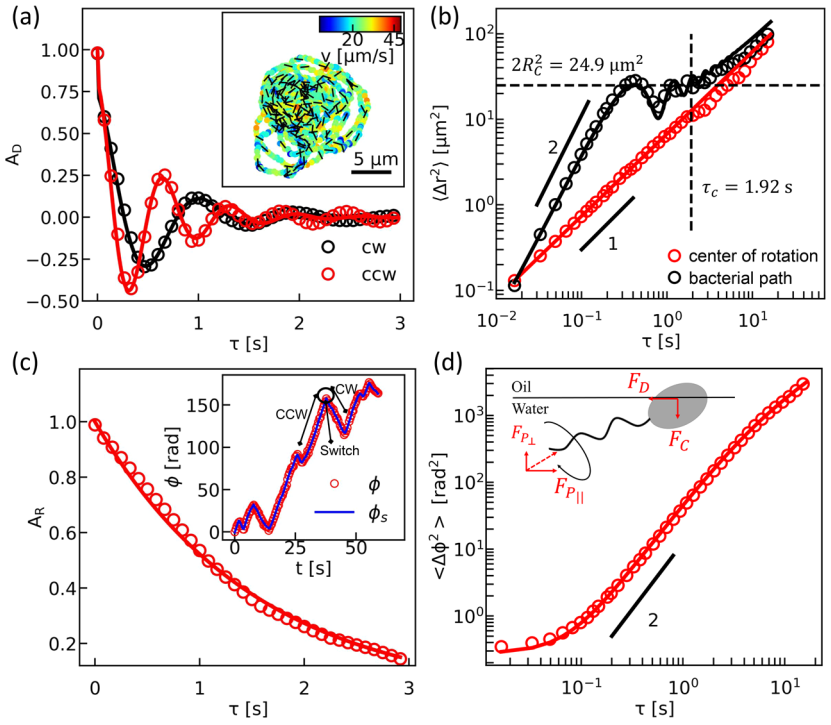


**Figure 6.** Translational and rotational behavior of an individual curly trajectory. (a) Directional autocorrelation function $A_D$ of CW, black circles, and CCW, red circles, segments of the trajectory with fits to eq 4. Inset: Trajectory over 30 s span colored by speed where the short black lines indicate the cell body orientation at every 10 frames. (b) MSD of the bacterial path, black circles, with fit to eq 6, black line. MSD of the center of the rotation, red circles, with a linear fit, red line. The black dashed line shows the subdiffusive plateau $2R_c^2$ and decorrelation time $\tau_c$ of the translational "self-caging" behavior. (c) Rotational autocorrelation function $A_R$, red circles, with exponential fit, red line. Inset: Instantaneous orientation and direction angle of a single trajectory. (d) MSAD, red circles, with red line fitted to eq 8. Inset: Schematic illustration of the bacterium with curly motion.

hook elasticity and cell rotational motion played a critical role in this process.[126] Our observations at the fluid interface might spur further research to relate the stability of this configuration to analysis and simulation of bacteria orientation near fluid boundaries, and the flexibility of the hook that connects the cell body to the motors that drive the flagellum.

**Curly Paths.** Bacteria swim in curly paths more than any other mode of motion; we see this mode for ∼40% of the individual bacteria over the first hour of the experiment, Figure 2e. These trajectories are quite stable; all curly trajectories persist over the observation period (60 s) except in the rare event that they collide with other bacteria and become trapped in a cluster. The trajectories have wide distributions of speed ($16.76 \pm 6.88\ \mu$m/s) and curvature ($0.33 \pm 0.3\ \mu m^{-1}$) (see Figure S3a,b for the probability distribution of speed and curvature). Segments of both CW and CCW circular paths are observed in the same trajectory. Based on the torque balance and drag asymmetry arguments, we assign CW segments to the pusher mode and CCW segments to the puller mode. Statistically, bacteria spend a random transit time in each mode with faster swimming speed and tighter circular path in puller (CCW) modes. Notably, changes between pusher and puller modes do not yield perfect reversals in direction; rather, the bacteria change direction with an angle distributed around 160°, as shown in Figure S 3d. This provides an important active mechanism for randomizing these trajectories. The transit times, the duration of "run" or "reverse" behavior, are distributed similarly, following an exponentially decay with a characteristic time of 1.1 s (Figure S3c).

The directional autocorrelation function $A_D$, Figure 6a, shows oscillatory behavior with exponential decaying amplitude, attributed to the curvilinear nature of the trajectories, and a sharp drop off between the first and second time points, attributable to passive Brownian diffusion. This motivates fitting these data to the functional form:

$$A_D(\tau) = \langle \boldsymbol{n}(t+\tau)\cdot\boldsymbol{n}(t)\rangle_t = \alpha \exp\left(-\frac{\tau}{\tau_{dif}}\right) + (1-\alpha)\exp\left(\frac{-\tau}{\tau_c}\right)\cos\left(\frac{2\pi\tau}{\tau_{osc}}\right) \quad (4)$$

The first term in eq 4 captures the importance of the short lag time Brownian diffusive processes; $\tau_{dif}$ is the directional decorrelation time owing to thermal diffusion. The second term reflects that the bacterium swims in circles, returning to its original direction after one period; $\tau_{osc}$ indicates the oscillation period. However, this circular swimming decorrelates over $\tau_c$ through active noisy processes, rather than thermal processes as was the case for the pirouettes. The fitted value for $\alpha$ is 0.25. The relative weight of the two terms reflects the relative importance of thermal and active motion.

The MSD of an individual curly trajectory is shown in Figure 6b; the MSD shows ballistic motion at early lag times. Oscillations about a subdiffusive plateau are also apparent in these curvilinear trajectories after a lag time of roughly 2 s. At long lag times, weak displacements of the center of the curvilinear motion ends the self-caging, after which the MSD becomes diffusive. The form of the directional autocorrelation function has implications for the form of the MSD, since the


https://dx.doi.org/10.1021/acs.langmuir.9b03578
Langmuir XXXX, XXX, XXX−XXX

MSD is related to its velocity autocorrelation function through the expression $\langle \Delta \boldsymbol{r}^2(\tau)\rangle = \int_0^\tau dt' \int_0^{t'} \langle \boldsymbol{v}(t)\cdot\boldsymbol{v}(t+t'')\rangle_t \, dt''$. If the swimming speed is assumed to be stationary and independent of the direction, the MSD can be estimated:

$$\langle \Delta \boldsymbol{r}^2(\tau)\rangle = 2\bar{v}^2 \int_0^\tau dt' \int_0^{t'} A_D(t'')\, dt'' \tag{5}$$

Substituting the expression for eq 4 into the above equation, the corresponding form for the MSD is

$$\langle \Delta \boldsymbol{r}^2(\tau)\rangle = 4(D_T + D_A)\tau + \frac{2R_c{}^2 c^2 (c^2-1)}{(1+c^2)^2} \times \left[\left(1 - e^{-\tau/\tau_c}\cos\frac{2\pi\tau}{\tau_{osc}}\right) + \frac{2c}{(1-c^2)} e^{-\tau/\tau_c}\sin\frac{2\pi\tau}{\tau_{osc}}\right] \tag{6}$$

where $c = 2\pi\tau_c/\tau_{osc}$ is the ratio of decorrelation time scale compared to the time to swim in a circle of radius $R_c$ (for details, see SI5). There are several signature behaviors that are captured in this expression. This expression has a familiar linear expression in lag time. This term has two contributions, Brownian diffusivity $D_T$ and an active diffusion term, allowing the active diffusion coefficient to be recognized as

$$4D_A = \frac{2\bar{v}^2\tau_c}{(1+c^2)} = \frac{2R_c{}^2}{\tau_c}\frac{c^2}{(1+c^2)} \approx \frac{2R_c{}^2}{\tau_c} \tag{7}$$

that captures the importance of $R_c$ as the length scale of the active processes and $\tau_c$ as the time scale for active noisy processes. The effective diffusivity measured for this curly trajectory is $D = D_T + D_A = 1.72\ \mu m^2/s$, an order of magnitude greater than that for thermal processes. Expanding eq 6 in powers of $\tau/\tau_c$ to quadratic order, the MSD is approximated as $\langle \Delta \boldsymbol{r}^2(\tau)\rangle \approx 4D_T\tau + \bar{v}^2\tau^2$.

Neglecting thermal diffusivity, the familiar ballistic regime is captured. Finally, the plateau in the MSD occurs for $\tau/\tau_c > 1$, with the prefactor giving the MSD value for the plateau. For this typical curly trajectory, the swimming direction decorrelates and becomes diffusive with a lag time of $\tau_c = 1.92$ s and the oscillation time $\tau_{osc} = 0.814$ s; thus, $c \gg 1$ and the prefactor to these terms can be approximated as $2R_c{}^2$. Thus, this functional form reveals that the plateau in MSD is given by the average square distance between two points randomly and uniformly distributed on a circle of radius $R_c$.

We also characterize the angular rotation in the interface by following changes in the angle $\phi$, which characterizes the orientation of the cell body during swimming, as shown in inset to Figure 6c. Here, we corrected the jumps between consecutive angles of directions and orientations by adding multiples of $\pm\pi$ to expand their range to $(-\infty, \infty)$ to capture continuous angular motion. We compare the body orientation to the swimming direction $\phi_s$ of the smoothed trajectories. As shown in the inset in Figure 6c, these two quantities nearly superpose, indicating that bacteria are swimming along their body axis, with intermittent change of swimming directions due to switches between pusher and puller modes. The angular rotation is highly deterministic, with linear changes in angle versus time in segments of run and reverse, indicating a constant rotational velocity in those segments of the trajectory. Superposed on this behavior, weak static noise is evident. To extract from these data rotational diffusion coefficients and characteristic rotational decorrelation times, we fitted the rotational autocorrelation function $A_R$ with exponential function: $A_R(\tau) = \exp(-\tau/\tau_R)$ and found decorrelation time $\tau_R = 2.13$ s, Figure 6c; a likely source of active decorrelation is the imperfect changes of direction between run and reverse. This form of the autocorrelation function also has implications for the mean-squared angular displacement. Assuming stationary rotational speed, the MSAD obeys $\langle \Delta\phi^2(\tau)\rangle = \bar{\Omega}^2 \int_0^\tau dt' \int_0^{t'} A_R(t'')\, dt''$, where $\bar{\Omega}$ indicates the mean angular velocity; the corresponding functional form for the MSAD is

$$\langle \Delta\phi^2(\tau)\rangle = 2D_R[\tau + \tau_R(e^{-\tau/\tau_R} - 1)] + 2\varepsilon_\phi{}^2 \tag{8}$$

where the constant term, $2\varepsilon_\phi{}^2$, has been added to capture the static noise. The MSAD for the curly trajectory shows ballistic behavior over a wide range of lag time (Figure 6d). At short lag time, the MSAD is nearly constant; this can be attributed to the noise in the orientation measurement. At very long lag times, we observe the signature of transition from ballistic to diffusive motion. By fitting eq 8 to the MSAD, we estimated the rotational decorrelation time to be $\tau_R = 2.13$ s, the static noise to be $\varepsilon_\phi = 0.366$ rad, and the rotational diffusion coefficient to be $D_R = 54\ rad^2/s$. This rotational diffusion coefficient is 2 orders of magnitude larger than that of Brownian diffusive bacterium, which is approximately $1.2\ rad^2/s$, and agrees nicely with the expected form for the active rotational diffusion coefficient $D_R = \bar{\Omega}^2\tau_R/2$ based on the angular velocity $\bar{\Omega} = 6.84$ rad/s measured from the angular orientation data and the rotational decorrelation time. Note that the characteristic rotational decorrelation time $\tau_R$ is similar in magnitude to the directional decorrelation time $\tau_c$, indicating possible hydrodynamic coupling between particle translation and rotation. To conclude, the preponderance of bacteria trapped at the fluid interface swim in curly motions that have active translation, active rotation, and active noise processes that result in active diffusion.

We infer an adsorbed state with the body adhered in an orientation tilted from the interfacial plane (inset to Figure 6d). The torque generated by the rotation of the flagellum must be balanced. The parallel component of this torque is balanced by the capillary torque and the normal component is balanced by rotational drag on the cell body. Therefore, when the flagellum is oriented normal to the interface (as in pirouettes), we observed fast rotation of the cell body. In the tilted configuration, however, only the normal component drives the counter rotation of the cell body. The cell body rotation accompanied by the propulsion force parallel to the interface leads to a curly motion. The body tilt angle determines the angle of the flagellum and hence the in-plane motion. The component of the propulsion force generated by the rotation of the flagellum parallel to the interface $F_{P\|}$ is balanced by the drag on the cell body, while interfacial trapping at the interface balances the propulsion force normal to the interface and prevents out of plane motion. The body tilt angle also alters the proximity of the flagellum to the interface. The drag on the parts of the flagellum close to the interface and the high viscosity oil phase is larger than that on the parts further from the interface, generating a hydrodynamic torque that reorients the whole bacteria leading to rotation around the $z$ axis.

To infer the tilt angle of cell body at interface, we have characterized the degree of elongation of the dark spot formed by the cell body in the interfacial plane by calculating its aspect ratio (length to width). The pirouettes are roughly circular in cross section with a mean aspect ratio of approximately 1.1 ±


https://dx.doi.org/10.1021/acs.langmuir.9b03578
Langmuir XXXX, XXX, XXX−XXX

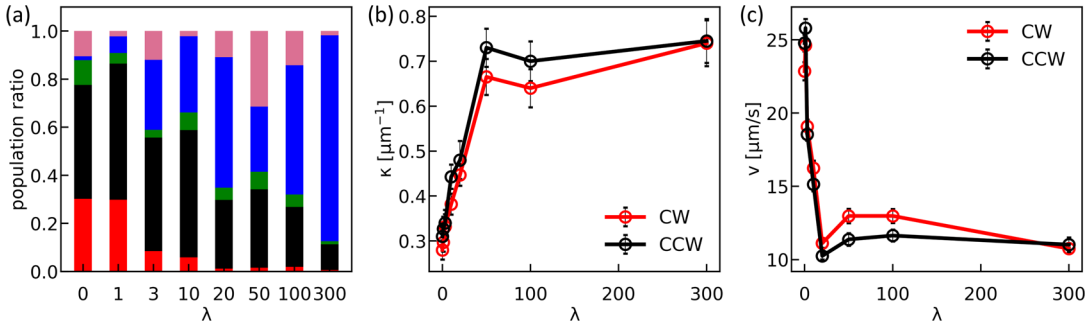


**Figure 7.** Motility is strongly changed by changes in superphase viscosity. (a) Population ratio of each trajectory type versus viscosity ratio. Curly motion: black; Brownian diffusive: blue; interfacial visitor: red; pirouette: green. Pink indicates fraction of clustered bacteria. Mean curvature (b) and mean speed (c) of CW and CCW segments of curly trajectories versus viscosity ratio.

0.05, suggesting a vertical alignment. The aspect ratio of bacteria with curly motion ranges from 1.1 to 1.9, with mean value 1.34 ± 0.15. Assuming that this range of aspect ratios corresponds to nearly vertical to nearly horizontal arrangements, the mean tilt angle can be inferred to be 66°. We propose that this range of tilt angle results from random contact line pinning. This pinning traps bacteria in random configurations. Thus, a single population of bacteria can generate a wide range of swimming behaviors.

Pili are known to play important roles in the behavior of bacteria near solid boundaries.[65,127] To probe whether pili play an important role in our system, we repeated the experiment for PA01 ΔpilC bacteria, which lack the gene for biosynthesis of pili. We observed the trajectory types for the bacteria for wild type and for the depilated bacteria for three experiments. The results are not significantly different from each other. Figure S6 shows an image of the interface for the depilated bacteria trajectories, and population distributions of each trajectory types. Similar to wild type PA01, the majority of ΔpilC cells are swimming in curly motion with similar curvatures and swimming velocities (Figure S6c).

**From Free Surfaces to Highly Viscous Adjacent Fluids.** To ascertain the role of the viscosity of the superphase, we study bacteria motion for different superphase fluids to span viscosity ratios $0 < \lambda < 300$, where $\lambda$ is defined as the ratio of superphase viscosity to subphase viscosity. Bacteria are first trapped on the air−water interface before we put the oil on top. All four types of motion are observed at interfaces for systems with various viscosity ratios. However, we also observe a transition from a predominantly active to a predominantly inert interface, as more bacteria become sessile with increased oil viscosity (Figure 7a). Analysis of curly motions for bacteria motion at aqueous−silicone oil interfaces shows that curvature increases with $\lambda$ and asymptotes for $\lambda > 50$ to a value of ∼0.7 $\mu m^{-1}$ (Figure 7b). This curvature value is an order of magnitude larger than that observed for bacteria swimming within 10 nm of a solid surface reported by Lauga et al.[92] Furthermore, the speed decreases simultaneously and asymptotes to 10 $\mu$m/s (Figure 7c). The low swimming speed is attributed to the large drag coefficient experienced from swimming on the interface and from partial immersion of the oil phase with large oil viscosity. This elevated drag is also revealed from the orders of magnitude decrease in the thermal diffusivity of the inert bacteria.

## CONCLUSION AND OUTLOOK

We have observed *P. aeruginosa* PA01, a motile bacterium that can switch between pusher and puller swimming modes, interacting with fluid interfaces. Two major bacterial populations are identified. Interface-visiting cells interact very close to the interface but can leave the interfacial region. These bacteria move ballistically along trajectories that are fully three-dimensional. The projected (2D) curvatures of these trajectories changes with distance from the interface without an accompanying change in swimming mode of bacteria, that is, a change between pusher and puller swimming. Their motion is not consistent with far-field analyses of bacteria near boundaries, which is likely due to their close proximity to the interface. Interfacially trapped cells do not escape from the interface. The preponderance of interfacially trapped bacteria swim with persistent curvilinear paths, in either curly or pirouette trajectories, that differ significantly from motions in the bulk. Interfacial trapping and dominance of surface tension over viscous stresses prevents the bacteria from deforming the fluid interface. We infer that the bacteria have pinned contact lines that prevent rotation except about the axis normal to the interface. Further, we infer that bacteria swimming with pirouette-type trajectories are trapped in near-perpendicular alignment to the interface. This alignment precludes in-plane active translation but allows rapid rotation and thermal diffusion of the bacteria cell body, which is consistent with our observations. We further infer that curly motions result from bacteria trapping at angles that are oblique or nearly parallel to the interface. These configurations would allow in-plane active translation and active rotation about axes perpendicular to the interface. Moreover, switching between swimming modes and other sources of active noise, contribute to active diffusion observed for curly trajectories.

There are a number of open issues worthy of detailed study motivated by these observations. It would be interesting to study in detail to behavior of swimmers adjacent to, but not adsorbed on, the fluid interface. However, the current system of PA01 is not suitable for this study. The bacteria PA01 frequently reverse their flagellar rotation, changing from pusher to puller swimming, and their rotational sense of their trajectories. This complicates the search for signature behaviors predicted in the hydrodynamic literature or new behaviors that have yet to be addressed. For example, a detailed discussion of the S-curve trajectories traced by some interfacial visitors will require extensive discussion in terms of hydrodynamic analysis. We will endeavor to probe this interesting phenomenon in future work on immersed bacteria


https://dx.doi.org/10.1021/acs.langmuir.9b03578
Langmuir XXXX, XXX, XXX−XXX

near interfaces using a system of swimmers that cannot reverse their swim direction.

While bacteria are known to adhere to hydrophobic interfaces,[128−130] the question of how the bacterium attaches to the interface also remains to be addressed. There is substantial literature on this issue for inert colloids adjacent to the interface in systems at rest, which interact energetically with the interface. Colloidal particles held in laser traps near interfaces can persist for extended periods of time without attaching, indicating the presence of the kinetic barriers.[131−135] Attachment occurs via a rapid snap-in event,[136,137] followed by rapid oscillations as the energy released by the attachment is dissipated. This energy is on the order of $10^7 kT$ for micrometer scale colloids, where $k$ is Boltzman's constant and $T$ is the temperature. The attachment energy includes contributions from the elimination of fluid−fluid interface and the satisfaction of wetting conditions on the particle and scales as the product of interfacial tension and the area of the hole made by the colloid in the interface.

After attachment, the contact lines on colloids move extremely slowly from one pinned state to another, with glassy dynamics, toward equilibrium.[131−133] Such detailed studies are lacking for particles near interfaces that are moving. However, it is known from emulsification studies that fluid motion promotes particle attachment and that, in general, solid particles have a high barrier to adsorption and to desorption.[138] We suspect that attachment occurs during the formation of the air−water interface, which is accompanied by significant motion. Notably, we do not observe attachment or detachment for any of the trajectories that we study. This may be because the unadhered, swimming bacteria do not remain very near the interface long enough to overcome the energy barriers to attachment. Future studies of the dynamics of bacteria attachment and a direct measurement of contact line pinning of bacteria cell bodies would be valuable.

This research also raises important questions about how fluid interfaces constrain bacterial motion and influence their behaviors through hydrodynamic and capillary forces. We infer that contact line pinning plays an important role in dictating the trajectories of bacteria, for example, by denying access to fuel for the Brownian diffusive bacteria or constraining the rotation of the cell body in the case of pirouettes and curly trajectories. Furthermore, the presence of the interface affects the fluid flows generated by the bacteria, a focus of ongoing work.

The role of active noise in generating the elevated diffusion of the curly swimmers leads to effective dispersal in this system. This dispersal occurred at sparse surface coverages of bacteria, for which hydrodynamic interactions are relatively weak. This finding might inspire research in the design of synthetic colloidal swimmers with active noisy mechanisms designed to enhance their dispersal. Finally, there has been tremendous interest in boundary guidance, for example, by shaping the diffusio-phoretic cloud of products behind catalytically powered active colloids that accumulate near solid boundaries. Trapping at fluid interfaces limits bacteria motion to the interfacial plane, a form of boundary guidance that could be combined with applied fields and other driving mechanisms to dictate active colloid path.

Finally, the mobility of fluid interfaces, in contrast to no-slip solid interfaces, means that these swimmers set up flows in the interface which translate to the surrounding fluid. Indeed, motion in the fluid adjacent to the interface has been reported at air−water interfaces for a pirouette-like adsorbed state.[118] It would be interesting to evaluate active sheets of bacteria swimming on fluid interfaces as a means of promoting transport. Furthermore, complex interfaces are the norm, including Marangoni effects that could resist active colloid motion. Proteins or other surface-active macromolecules can impart surface viscous effects with associated long-ranged decay of the interfacial flows. These are topics of ongoing research.

## ■ ASSOCIATED CONTENT

### Supporting Information

The Supporting Information is available free of charge at https://pubs.acs.org/doi/10.1021/acs.langmuir.9b03578.

Description of modeling of bounded rotational mean squared displacement of bacteria; example trajectories of visitor bacteria; more information about motility characteristics of the bacteria with curly paths; directional and rotational autocorrelation functions and the MSD of a curvilinear path; result for PA01 ΔpilC (PDF)

Interfacial visitor bacterium I (AVI)

Interfacial visitor bacterium II (AVI)

Immotile bacterium moving via Brownian diffusion bacterium (AVI)

Bacterium with a pirouette motion (AVI)

Bacterium swimming in a curly path (AVI)

## ■ AUTHOR INFORMATION


### Corresponding Author

**Kathleen J. Stebe** − *Department of Chemical and Biomolecular Engineering, University of Pennsylvania, Philadelphia, United States;* orcid.org/0000-0003-0510-0513; Email: kstebe@seas.upenn.edu

### Authors

**Jiayi Deng** − *Department of Chemical and Biomolecular Engineering, University of Pennsylvania, Philadelphia, United States*

**Mehdi Molaei** − *Department of Chemical and Biomolecular Engineering, University of Pennsylvania, Philadelphia, United States*

**Nicholas G. Chisholm** − *Department of Chemical and Biomolecular Engineering, University of Pennsylvania, Philadelphia, United States*

Complete contact information is available at: https://pubs.acs.org/10.1021/acs.langmuir.9b03578


### Author Contributions

†J.D. and M.M. contributed equally to this work.

### Notes

The authors declare no competing financial interest.

## ■ ACKNOWLEDGMENTS

The authors acknowledge support for N.G.C. and M.M. from NSF-DMR 1607878 and for J.D. from a grant through The Gulf of Mexico Research Initiative. Data are publicly available through the Gulf of Mexico Research Initiative Information and Data Cooperative (GRIIDC) at https://data.gulfresearchinitiative.org.



https://dx.doi.org/10.1021/acs.langmuir.9b03578
Langmuir XXXX, XXX, XXX−XXX

## REFERENCES


(1) Ebbens, S. Active colloids: Progress and challenges towards realising autonomous applications. *Curr. Opin. Colloid Interface Sci.* **2016**, *21*, 14−23.
(2) Zhao, X.; Gentile, K.; Mohajerani, F.; Sen, A. Powering Motion with Enzymes. *Acc. Chem. Res.* **2018**, *51*, 2373−2381.
(3) Vaccari, L.; Molaei, M.; Leheny, R. L.; Stebe, K. J. Cargo carrying bacteria at interfaces. *Soft Matter* **2018**, *14*, 5643−5653.
(4) Wong, D.; Beattie, E. E.; Steager, E. B.; Kumar, V. Effect of surface interactions and geometry on the motion of micro bio robots. *Appl. Phys. Lett.* **2013**, *103*, 153707.
(5) Behkam, B.; Sitti, M. Effect of quantity and configuration of attached bacteria on bacterial propulsion of microbeads. *Appl. Phys. Lett.* **2008**, *93*, 223901.
(6) Martel, S. Bacterial microsystems and microrobots. *Biomed. Microdevices* **2012**, *14*, 1033−1045.
(7) Steager, E.; Kim, C.-B.; Patel, J.; Bith, S.; Naik, C.; Reber, L.; Kim, M. J. Control of microfabricated structures powered by flagellated bacteria using phototaxis. *Appl. Phys. Lett.* **2007**, *90*, 263901.
(8) Edwards, M. R.; Wright Carlsen, R.; Sitti, M. Near and far-wall effects on the three-dimensional motion of bacteria-driven microbeads. *Appl. Phys. Lett.* **2013**, *102*, 143701.
(9) Stanton, M. M.; Park, B.-W.; Miguel-López, A.; Ma, X.; Sitti, M.; Sánchez, S. Biohybrid Microtube Swimmers Driven by Single Captured Bacteria. *Small* **2017**, *13*, 1603679.
(10) Alapan, Y.; Yasa, O.; Yigit, B.; Yasa, I. C.; Erkoc, P.; Sitti, M. Microrobotics and Microorganisms: Biohybrid Autonomous Cellular Robots. *Annual Review of Control, Robotics, and Autonomous Systems* **2019**, *2*, 205−230.
(11) Zhu, S.; Schniederberend, M.; Zhitnitsky, D.; Jain, R.; Galán, J. E.; Kazmierczak, B. I.; Liu, J. *In Situ* Structures of Polar and Lateral Flagella Revealed by Cryo-Electron Tomography. *J. Bacteriol.* **2019**, *201*, e00117-19.
(12) Minamino, T.; Imada, K.; Namba, K. Molecular motors of the bacterial flagella. *Curr. Opin. Struct. Biol.* **2008**, *18*, 693−701.
(13) Jawed, M.; Khouri, N.; Da, F.; Grinspun, E.; Reis, P. Propulsion and Instability of a Flexible Helical Rod Rotating in a Viscous Fluid. *Phys. Rev. Lett.* **2015**, *115*, 168101.
(14) Nguyen, F. T. M.; Graham, M. D. Impacts of multiflagellarity on stability and speed of bacterial locomotion. *Phys. Rev. E: Stat. Phys., Plasmas, Fluids, Relat. Interdiscip. Top.* **2018**, *98*, 042419.
(15) Wu, W.; Jin, Y.; Bai, F.; Jin, S. In *Molecular Medical Microbiology*, Second ed.; Tang, Y.-W., Sussman, M., Liu, D., Poxton, I., Schwartzman, J., Eds.; Academic Press: Boston, 2015; pp 753−767.
(16) Chang, C.-Y. Surface Sensing for Biofilm Formation in Pseudomonas aeruginosa. *Front. Microbiol.* **2018**, *8*, 2671.
(17) Bruinsma, G. M.; Rustema-Abbing, M.; van der Mei, H. C.; Busscher, H. J. Effects of cell surface damage on surface properties and adhesion of Pseudomonas aeruginosa. *J. Microbiol. Methods* **2001**, *45*, 95−101.
(18) Qian, C.; Wong, C. C.; Swarup, S.; Chiam, K.-H. Bacterial Tethering Analysis Reveals a "Run-Reverse-Turn" Mechanism for Pseudomonas Species Motility. *Appl. Environ. Microbiol.* **2013**, *79*, 4734−4743.
(19) Cai, Q.; Li, Z.; Ouyang, Q.; Luo, C.; Gordon, V. D. Singly Flagellated *Pseudomonas aeruginosa* Chemotaxes Efficiently by Unbiased Motor Regulation. *mBio* **2016**, *7*, e00013-16.
(20) Taylor, B. L.; Koshland, D. E. Reversal of Flagellar Rotation in Monotrichous and Peritrichous Bacteria: Generation of Changes in Direction. *J. Bacteriol.* **1974**, *119*, 640−642.
(21) Xie, L.; Altindal, T.; Chattopadhyay, S.; Wu, X.-L. Bacterial flagellum as a propeller and as a rudder for efficient chemotaxis. *Proc. Natl. Acad. Sci. U. S. A.* **2011**, *108*, 2246−2251.
(22) Son, K.; Guasto, J. S.; Stocker, R. Bacteria can exploit a flagellar buckling instability to change direction. *Nat. Phys.* **2013**, *9*, 494−498.
(23) Fei, W.; Gu, Y.; Bishop, K. J. Active colloidal particles at fluid-fluid interfaces. *Curr. Opin. Colloid Interface Sci.* **2017**, *32*, 57−68.
(24) Brennen, C.; Winet, H. Fluid Mechanics of Propulsion by Cilia and Flagella. *Annu. Rev. Fluid Mech.* **1977**, *9*, 339−398.
(25) Pedley, T. J.; Kessler, J. O. Hydrodynamic Phenomena in Suspensions of Swimming Microorganisms. *Annu. Rev. Fluid Mech.* **1992**, *24*, 313−358.
(26) Wu, X.-L.; Libchaber, A. Particle Diffusion in a Quasi-Two-Dimensional Bacterial Bath. *Phys. Rev. Lett.* **2000**, *84*, 3017−3020.
(27) Lauga, E.; Powers, T. R. The hydrodynamics of swimming microorganisms. *Rep. Prog. Phys.* **2009**, *72*, 096601.
(28) Lauga, E. Bacterial Hydrodynamics. *Annu. Rev. Fluid Mech.* **2016**, *48*, 105−130.
(29) Drescher, K.; Goldstein, R. E.; Michel, N.; Polin, M.; Tuval, I. Direct Measurement of the Flow Field around Swimming Microorganisms. *Phys. Rev. Lett.* **2010**, *105*, 168101.
(30) Drescher, K.; Dunkel, J.; Cisneros, L. H.; Ganguly, S.; Goldstein, R. E. Fluid dynamics and noise in bacterial cell−cell and cell−surface scattering. *Proc. Natl. Acad. Sci. U. S. A.* **2011**, *108*, 10940−10945.
(31) Ishikawa, T.; Simmonds, M. P.; Pedley, T. J. Hydrodynamic interaction of two swimming model micro-organisms. *J. Fluid Mech.* **2006**, *568*, 119.
(32) Ishikawa, T.; Sekiya, G.; Imai, Y.; Yamaguchi, T. Hydrodynamic interactions between two swimming bacteria. *Biophys. J.* **2007**, *93*, 2217−2225.
(33) Lauga, E.; Goldstein, R. E. Dance of the microswimmers. *Phys. Today* **2012**, *65*, 30.
(34) Hernandez-Ortiz, J. P.; Stoltz, C. G.; Graham, M. D. Transport and Collective Dynamics in Suspensions of Confined Swimming Particles. *Phys. Rev. Lett.* **2005**, *95*, 204501.
(35) Cisneros, L. H.; Cortez, R.; Dombrowski, C.; Goldstein, R. E.; Kessler, J. O. Fluid dynamics of self-propelled microorganisms, from individuals to concentrated populations. *Exp. Fluids* **2007**, *43*, 737−753.
(36) Underhill, P. T.; Hernandez-Ortiz, J. P.; Graham, M. D. Diffusion and Spatial Correlations in Suspensions of Swimming Particles. *Phys. Rev. Lett.* **2008**, *100*, 248101.
(37) Baskaran, A.; Marchetti, M. C. Statistical mechanics and hydrodynamics of bacterial suspensions. *Proc. Natl. Acad. Sci. U. S. A.* **2009**, *106*, 15567−15572.
(38) Pedley, T. J. Collective Behaviour of Swimming Microorganisms. *Exp. Mech.* **2010**, *50*, 1293−1301.
(39) Cisneros, L. H.; Kessler, J. O.; Ganguly, S.; Goldstein, R. E. Dynamics of swimming bacteria: Transition to directional order at high concentration. *Phys. Rev. E* **2011**, *83*, 061907.
(40) Ishikawa, T.; Pedley, T. J. Coherent Structures in Monolayers of Swimming Particles. *Phys. Rev. Lett.* **2008**, *100*, 088103.
(41) Ishikawa, T. Suspension biomechanics of swimming microbes. *J. R. Soc., Interface* **2009**, *6*, 815−834.
(42) Ishikawa, T.; Locsei, J. T.; Pedley, T. J. Fluid particle diffusion in a semidilute suspension of model micro-organisms. *Phys. Rev. E* **2010**, *82*, 021408.
(43) Ishikawa, T. Models and Numerical Methods for a Suspension of Swimming Microorganisms: Review. *Int. J. Offshore Polar Eng.* **2012**, *22*, 270−275.
(44) Saintillan, D.; Shelley, M. J. Active suspensions and their nonlinear models. *C. R. Phys.* **2013**, *14*, 497−517.
(45) Takatori, S. C.; De Dier, R.; Vermant, J.; Brady, J. F. Acoustic trapping of active matter. *Nat. Commun.* **2016**, *7*, 10694.
(46) Sokolov, A.; Aranson, I. S.; Kessler, J. O.; Goldstein, R. E. Concentration Dependence of the Collective Dynamics of Swimming Bacteria. *Phys. Rev. Lett.* **2007**, *98*, 158102.
(47) Koch, D. L.; Subramanian, G. Collective Hydrodynamics of Swimming Microorganisms: Living Fluids. *Annu. Rev. Fluid Mech.* **2011**, *43*, 637−659.
(48) Fily, Y.; Marchetti, M. C. Athermal Phase Separation of Self-Propelled Particles with No Alignment. *Phys. Rev. Lett.* **2012**, *108*, 235702.
(49) Fily, Y.; Henkes, S.; Marchetti, M. C. Freezing and phase separation of self-propelled disks. *Soft Matter* **2014**, *10*, 2132−2140.



https://dx.doi.org/10.1021/acs.langmuir.9b03578
*Langmuir* XXXX, XXX, XXX−XXX

(50) Burkholder, E. W.; Brady, J. F. Tracer diffusion in active suspensions. *Phys. Rev. E: Stat. Phys., Plasmas, Fluids, Relat. Interdiscip. Top.* **2017**, *95*, 052605.
(51) Burkholder, E. W.; Brady, J. F. Fluctuation-dissipation in active matter. *J. Chem. Phys.* **2019**, *150*, 184901.
(52) Banerjee, D.; Souslov, A.; Abanov, A. G.; Vitelli, V. Odd viscosity in chiral active fluids. *Nat. Commun.* **2017**, *8*, 1573.
(53) Kaya, T.; Koser, H. Direct Upstream Motility in Escherichia coli. *Biophys. J.* **2012**, *102*, 1514−1523.
(54) Hill, J.; Kalkanci, O.; McMurry, J. L.; Koser, H. Hydrodynamic Surface Interactions Enable Escherichia Coli to Seek Efficient Routes to Swim Upstream. *Phys. Rev. Lett.* **2007**, *98*, 068101.
(55) Marcos; Fu, H. C.; Powers, T. R.; Stocker, R. Bacterial rheotaxis. *Proc. Natl. Acad. Sci. U. S. A.* **2012**, *109*, 4780−4785.
(56) Molaei, M.; Sheng, J. Succeed escape: Flow shear promotes tumbling of Escherichia colinear a solid surface. *Sci. Rep.* **2016**, *6*, 35290.
(57) Wilson, L. G.; Martinez, V. A.; Schwarz-Linek, J.; Tailleur, J.; Bryant, G.; Pusey, P. N.; Poon, W. C. K. Differential Dynamic Microscopy of Bacterial Motility. *Phys. Rev. Lett.* **2011**, *106*, 018101.
(58) Martinez, V.; Besseling, R.; Croze, O.; Tailleur, J.; Reufer, M.; Schwarz-Linek, J.; Wilson, L.; Bees, M.; Poon, W. K. Differential Dynamic Microscopy: A High-Throughput Method for Characterizing the Motility of Microorganisms. *Biophys. J.* **2012**, *103*, 1637−1647.
(59) Berke, A. P.; Turner, L.; Berg, H. C.; Lauga, E. Hydrodynamic Attraction of Swimming Microorganisms by Surfaces. *Phys. Rev. Lett.* **2008**, *101*, 038102.
(60) Takatori, S. C.; Brady, J. F. Forces, stresses and the (thermo?) dynamics of active matter. *Curr. Opin. Colloid Interface Sci.* **2016**, *21*, 24−33.
(61) Schaar, K.; Zöttl, A.; Stark, H. Detention Times of Microswimmers Close to Surfaces: Influence of Hydrodynamic Interactions and Noise. *Phys. Rev. Lett.* **2015**, *115*, 038101.
(62) Bianchi, S.; Saglimbeni, F.; Di Leonardo, R. Holographic Imaging Reveals the Mechanism of Wall Entrapment in Swimming Bacteria. *Phys. Rev. X* **2017**, *7*, 011010.
(63) Qi, M.; Gong, X.; Wu, B.; Zhang, G. Landing Dynamics of Swimming Bacteria on a Polymeric Surface: Effect of Surface Properties. *Langmuir* **2017**, *33*, 3525−3533.
(64) Hu, J.; Wysocki, A.; Winkler, R. G.; Gompper, G. Physical Sensing of Surface Properties by Microswimmers − Directing Bacterial Motion via Wall Slip. *Sci. Rep.* **2015**, *5*, 9586.
(65) Utada, A. S.; Bennett, R. R.; Fong, J. C. N.; Gibiansky, M. L.; Yildiz, F. H.; Golestanian, R.; Wong, G. C. L. Vibrio cholerae use pili and flagella synergistically to effect motility switching and conditional surface attachment. *Nat. Commun.* **2014**, *5*, 4913.
(66) de Anda, J.; Lee, E. Y.; Lee, C. K.; Bennett, R. R.; Ji, X.; Soltani, S.; Harrison, M. C.; Baker, A. E.; Luo, Y.; Chou, T.; O'Toole, G. A.; Armani, A. M.; Golestanian, R.; Wong, G. C. L. High-Speed "4D" Computational Microscopy of Bacterial Surface Motility. *ACS Nano* **2017**, *11*, 9340−9351.
(67) Tran, V. B.; Fleiszig, S. M. J.; Evans, D. J.; Radke, C. J. Dynamics of Flagellum- and Pilus-Mediated Association of Pseudomonas aeruginosa with Contact Lens Surfaces. *Appl. Environ. Microbiol.* **2011**, *77*, 3644−3652.
(68) Kühn, M. J.; Schmidt, F. K.; Eckhardt, B.; Thormann, K. M. Bacteria exploit a polymorphic instability of the flagellar filament to escape from traps. *Proc. Natl. Acad. Sci. U. S. A.* **2017**, *114*, 6340−6345.
(69) Mathijssen, A. J. T. M.; Guzman-Lastra, F.; Kaiser, A.; Lowen, H. Nutrient Transport Driven by Microbial Active Carpets. *Phys. Rev. Lett.* **2018**, *121*, 248101.
(70) Darnton, N.; Turner, L.; Breuer, K.; Berg, H. C. Moving Fluid with Bacterial Carpets. *Biophys. J.* **2004**, *86*, 1863−1870.
(71) Kim, M.; Breuer, K. Microfluidic Pump Powered by Self-Organizing Bacteria. *Small* **2008**, *4*, 111−118.
(72) Hall-Stoodley, L.; Costerton, J. W.; Stoodley, P. Bacterial biofilms: from the natural environment to infectious diseases. *Nat. Rev. Microbiol.* **2004**, *2*, 95−108.
(73) Donlan, R. M. Biofilms: microbial life on surfaces. *Emerging Infect. Dis.* **2002**, *8*, 881−890.
(74) O'Toole, G.; Kaplan, H. B.; Kolter, R. Biofilm Formation as Microbial Development. *Annu. Rev. Microbiol.* **2000**, *54*, 49−79.
(75) Costerton, J. W.; Stewart, P. S.; Greenberg, E. P. Bacterial Biofilms: A Common Cause of Persistent Infections. *Science* **1999**, *284*, 1318−1322.
(76) Flemming, H.-C.; Wingender, J.; Szewzyk, U.; Steinberg, P.; Rice, S. A.; Kjelleberg, S. Biofilms: an emergent form of bacterial life. *Nat. Rev. Microbiol.* **2016**, *14*, 563−575.
(77) Conrad, J. C.; Poling-Skutvik, R. Confined Flow: Consequences and Implications for Bacteria and Biofilms. *Annu. Rev. Chem. Biomol. Eng.* **2018**, *9*, 175−200.
(78) Gordon, V. D.; Davis-Fields, M.; Kovach, K.; Rodesney, C. A. Biofilms and mechanics: a review of experimental techniques and findings. *J. Phys. D: Appl. Phys.* **2017**, *50*, 223002.
(79) Garrett, T. R.; Bhakoo, M.; Zhang, Z. Bacterial adhesion and biofilms on surfaces. *Prog. Nat. Sci.* **2008**, *18*, 1049−1056.
(80) Tuson, H. H.; Weibel, D. B. Bacteria−surface interactions. *Soft Matter* **2013**, *9*, 4368.
(81) Dunne, W. M. Bacterial Adhesion: Seen Any Good Biofilms Lately? *Clin. Microbiol. Rev.* **2002**, *15*, 155−166.
(82) Vaccari, L.; Allan, D. B.; Sharifi-Mood, N.; Singh, A. R.; Leheny, R. L.; Stebe, K. J. Films of bacteria at interfaces: three stages of behaviour. *Soft Matter* **2015**, *11*, 6062−6074.
(83) Vaccari, L.; Molaei, M.; Niepa, T. H. R.; Lee, D.; Leheny, R. L.; Stebe, K. J. Films of bacteria at interfaces. *Adv. Colloid Interface Sci.* **2017**, *247*, 561−572.
(84) Niepa, T. H. R.; Vaccari, L.; Leheny, R. L.; Goulian, M.; Lee, D.; Stebe, K. J. Films of Bacteria at Interfaces (FBI): Remodeling of Fluid Interfaces by Pseudomonas aeruginosa. *Sci. Rep.* **2017**, *7*, 17864.
(85) Giacché, D.; Ishikawa, T.; Yamaguchi, T. Hydrodynamic entrapment of bacteria swimming near a solid surface. *Phys. Rev. E* **2010**, *82*, 056309.
(86) Shum, H.; Gaffney, E. A.; Smith, D. J. Modelling bacterial behaviour close to a no-slip plane boundary: the influence of bacterial geometry. *Proc. R. Soc. London, Ser. A* **2010**, *466*, 1725−1748.
(87) Li, G.; Tang, J. X. Accumulation of Microswimmers near a Surface Mediated by Collision and Rotational Brownian Motion. *Phys. Rev. Lett.* **2009**, *103*, 078101.
(88) Li, G.; Tam, L.-K.; Tang, J. X. Amplified effect of Brownian motion in bacterial near-surface swimming. *Proc. Natl. Acad. Sci. U. S. A.* **2008**, *105*, 18355−18359.
(89) Wu, K.-T.; Hsiao, Y.-T.; Woon, W.-Y. Entrapment of pusher and puller bacteria near a solid surface. *Phys. Rev. E: Stat. Phys., Plasmas, Fluids, Relat. Interdiscip. Top.* **2018**, *98*, 052407.
(90) Lushi, E.; Kantsler, V.; Goldstein, R. E. Scattering of biflagellate microswimmers from surfaces. *Phys. Rev. E: Stat. Phys., Plasmas, Fluids, Relat. Interdiscip. Top.* **2017**, *96*, 023102.
(91) Molaei, M.; Barry, M.; Stocker, R.; Sheng, J. Failed Escape: Solid Surfaces Prevent Tumbling of 9. *Phys. Rev. Lett.* **2014**, *113*, 038103.
(92) Lauga, E.; DiLuzio, W. R.; Whitesides, G. M.; Stone, H. A. Swimming in Circles: Motion of Bacteria near Solid Boundaries. *Biophys. J.* **2006**, *90*, 400−412.
(93) Molaei, M.; Sheng, J. Imaging bacterial 3D motion using digital in-line holographic microscopy and correlation-based de-noising algorithm. *Opt. Express* **2014**, *22*, 32119−32137.
(94) Frymier, P. D.; Ford, R. M.; Berg, H. C.; Cummings, P. T. Three-dimensional tracking of motile bacteria near a solid planar surface. *Proc. Natl. Acad. Sci. U. S. A.* **1995**, *92*, 6195−6199.
(95) Ramia, M.; Tullock, D. L.; Phan-Thien, N. The role of hydrodynamic interaction in the locomotion of microorganisms. *Biophys. J.* **1993**, *65*, 755−778.


https://dx.doi.org/10.1021/acs.langmuir.9b03578
*Langmuir* XXXX, XXX, XXX−XXX

(96) Kudo, S.; Imai, N.; Nishitoba, M.; Sugiyama, S.; Magariyama, Y. Asymmetric swimming pattern of *Vibrio alginolyticus* cells with single polar flagella. *FEMS Microbiol. Lett.* **2005**, *242*, 221−225.
(97) Magariyama, Y.; Ichiba, M.; Nakata, K.; Baba, K.; Ohtani, T.; Kudo, S.; Goto, T. Difference in Bacterial Motion between Forward and Backward Swimming Caused by the Wall Effect. *Biophys. J.* **2005**, *88*, 3648−3658.
(98) Ping, L.; Birkenbeil, J.; Monajembashi, S. Swimming behavior of the monotrichous bacterium *Pseudomonas fluorescens* SBW25. *FEMS Microbiol. Ecol.* **2013**, *86*, 36−44.
(99) Howse, J. R.; Jones, R. A. L.; Ryan, A. J.; Gough, T.; Vafabakhsh, R.; Golestanian, R. Self-Motile Colloidal Particles: From Directed Propulsion to Random Walk. *Phys. Rev. Lett.* **2007**, *99*, 048102.
(100) Romanczuk, P.; Bär, M.; Ebeling, W.; Lindner, B.; Schimansky-Geier, L. Active Brownian particles. *Eur. Phys. J.: Spec. Top.* **2012**, *202*, 1−162.
(101) Großmann, R.; Peruani, F.; Bär, M. Diffusion properties of active particles with directional reversal. *New J. Phys.* **2016**, *18*, 043009.
(102) Detcheverry, F. Non-Poissonian run-and-turn motions. *EPL (Europhysics Letters)* **2015**, *111*, 60002.
(103) Mathijssen, A. J. T. M.; Pushkin, D. O.; Yeomans, J. M. Tracer trajectories and displacement due to a micro-swimmer near a surface. *J. Fluid Mech.* **2015**, *773*, 498−519.
(104) Petroff, A. P.; Wu, X.-L.; Libchaber, A. Fast-Moving Bacteria Self-Organize into Active Two-Dimensional Crystals of Rotating Cells. *Phys. Rev. Lett.* **2015**, *114*, 158102.
(105) Petroff, A. P.; Libchaber, A. Nucleation of rotating crystals by *Thiovulum majus* bacteria. *New J. Phys.* **2018**, *20*, 015007.
(106) Das, D.; Lauga, E. Transition to bound states for bacteria swimming near surfaces. *arXiv* (Fluid Dynamics), October 2, 2019, 1910.01502, ver. 1.
(107) Mozaffari, A.; Sharifi-Mood, N.; Koplik, J.; Maldarelli, C. Self-propelled colloidal particle near a planar wall: A Brownian dynamics study. *Physical Review Fluids* **2018**, *3*, 014104.
(108) Das, S.; Garg, A.; Campbell, A. I.; Howse, J.; Sen, A.; Velegol, D.; Golestanian, R.; Ebbens, S. J. Boundaries can steer active Janus spheres. *Nat. Commun.* **2015**, *6*, 8999.
(109) Di Leonardo, R.; Dell'Arciprete, D.; Angelani, L.; Iebba, V. Swimming with an Image. *Phys. Rev. Lett.* **2011**, *106*, 038101.
(110) Bianchi, S.; Saglimbeni, F.; Frangipane, G.; Dell'Arciprete, D.; Di Leonardo, R. 3D dynamics of bacteria wall entrapment at a water−air interface. *Soft Matter* **2019**, *15*, 3397−3406.
(111) Lemelle, L.; Palierne, J.-F.; Chatre, E.; Place, C. Counter-clockwise Circular Motion of Bacteria Swimming at the Air-Liquid Interface. *J. Bacteriol.* **2010**, *192*, 6307−6308.
(112) Morse, M.; Huang, A.; Li, G.; Maxey, M.; Tang, J. Molecular Adsorption Steers Bacterial Swimming at the Air/Water Interface. *Biophys. J.* **2013**, *105*, 21−28.
(113) Wang, X.; In, M.; Blanc, C.; Nobili, M.; Stocco, A. Enhanced active motion of Janus colloids at the water surface. *Soft Matter* **2015**, *11*, 7376−7384.
(114) Dietrich, K.; Renggli, D.; Zanini, M.; Volpe, G.; Buttinoni, I.; Isa, L. Two-dimensional nature of the active Brownian motion of catalytic microswimmers at solid and liquid interfaces. *New J. Phys.* **2017**, *19*, 065008.
(115) Dietrich, K.; Volpe, G.; Sulaiman, M. N.; Renggli, D.; Buttinoni, I.; Isa, L. Active Atoms and Interstitials in Two-Dimensional Colloidal Crystals. *Phys. Rev. Lett.* **2018**, *120*, 268004.
(116) Wang, X.; In, M.; Blanc, C.; Würger, A.; Nobili, M.; Stocco, A. Janus Colloids Actively Rotating on the Surface of Water. *Langmuir* **2017**, *33*, 13766−13773.
(117) Kümmel, F.; ten Hagen, B.; Wittkowski, R.; Buttinoni, I.; Eichhorn, R.; Volpe, G.; Löwen, H.; Bechinger, C. Circular Motion of Asymmetric Self-Propelling Particles. *Phys. Rev. Lett.* **2013**, *110*, 198302.
(118) Chen, X.; Yang, X.; Yang, M.; Zhang, H. P. Dynamic clustering in suspension of motile bacteria. *EPL (Europhysics Letters)* **2015**, *111*, 54002.
(119) Archer, R. J.; Campbell, A. I.; Ebbens, S. J. Glancing angle metal evaporation synthesis of catalytic swimming Janus colloids with well defined angular velocity. *Soft Matter* **2015**, *11*, 6872−6880.
(120) Campbell, A. I.; Wittkowski, R.; ten Hagen, B.; Löwen, H.; Ebbens, S. J. Helical paths, gravitaxis, and separation phenomena for mass-anisotropic self-propelling colloids: Experiment versus theory. *J. Chem. Phys.* **2017**, *147*, 084905.
(121) Ebbens, S. J.; Gregory, D. A. Catalytic Janus Colloids: Controlling Trajectories of Chemical Microswimmers. *Acc. Chem. Res.* **2018**, *51*, 1931−1939.
(122) Lisicki, M.; Reigh, S. Y.; Lauga, E. Autophoretic motion in three dimensions. *Soft Matter* **2018**, *14*, 3304−3314.
(123) Crocker, J. C.; Grier, D. G. Methods of Digital Video Microscopy for Colloidal Studies. *J. Colloid Interface Sci.* **1996**, *179*, 298−310.
(124) Molaei, M.; Atefi, E.; Crocker, J. C. Nanoscale Rheology and Anisotropic Diffusion Using Single Gold Nanorod Probes. *Phys. Rev. Lett.* **2018**, *120*, 118002.
(125) Lopez, D.; Lauga, E. Dynamics of swimming bacteria at complex interfaces. *Phys. Fluids* **2014**, *26*, 071902.
(126) Ishimoto, K. Bacterial spinning top. *J. Fluid Mech.* **2019**, *880*, 620−652.
(127) Golovkine, G.; Lemelle, L.; Burny, C.; Vaillant, C.; Palierne, J.-F.; Place, C.; Huber, P. Host cell surfaces induce a Type IV pili-dependent alteration of bacterial swimming. *Sci. Rep.* **2016**, *6*, 38950.
(128) Dewangan, N. K.; Conrad, J. C. Adhesion of *Marinobacter hydrocarbonoclasticus* to Surfactant-Decorated Dodecane Droplets. *Langmuir* **2018**, *34*, 14012−14021.
(129) Doyle, R. J.; Rosenberg, M. *Methods in Enzymology*; Elsevier, 1995; Vol. *253*; pp 542−550.
(130) Rühs, P.; Böcker, L.; Inglis, R.; Fischer, P. Studying bacterial hydrophobicity and biofilm formation at liquid−liquid interfaces through interfacial rheology and pendant drop tensiometry. *Colloids Surf., B* **2014**, *117*, 174−184.
(131) Kaz, D. M.; McGorty, R.; Mani, M.; Brenner, M. P.; Manoharan, V. N. Physical ageing of the contact line on colloidal particles at liquid interfaces. *Nat. Mater.* **2012**, *11*, 138−142.
(132) Wang, A.; McGorty, R.; Kaz, D. M.; Manoharan, V. N. Contact-line pinning controls how quickly colloidal particles equilibrate with liquid interfaces. *Soft Matter* **2016**, *12*, 8958−8967.
(133) Colosqui, C. E.; Morris, J. F.; Koplik, J. Colloidal Adsorption at Fluid Interfaces: Regime Crossover from Fast Relaxation to Physical Aging. *Phys. Rev. Lett.* **2013**, *111*, 028302.
(134) Rahmani, A. M.; Wang, A.; Manoharan, V. N.; Colosqui, C. E. Colloidal particle adsorption at liquid interfaces: capillary driven dynamics and thermally activated kinetics. *Soft Matter* **2016**, *12*, 6365−6372.
(135) Wang, A.; Kaz, D. M.; McGorty, R.; Manoharan, V. N. Relaxation dynamics of colloidal particles at liquid interfaces. *AIP Conf. Proc.* **2013**, 336−343.
(136) Chen, L.; Heim, L.-O.; Golovko, D. S.; Bonaccurso, E. Snap-in dynamics of single particles to water drops. *Appl. Phys. Lett.* **2012**, *101*, 031601.
(137) Singh, P.; Joseph, D. D.; Gurupatham, S. K.; Dalal, B.; Nudurupati, S. Spontaneous dispersion of particles on liquid surfaces. *Proc. Natl. Acad. Sci. U. S. A.* **2009**, *106*, 19761−19764.
(138) Tcholakova, S.; Denkov, N. D.; Lips, A. Comparison of solid particles, globular proteins and surfactants as emulsifiers. *Phys. Chem. Chem. Phys.* **2008**, *10*, 1608−1627.


https://dx.doi.org/10.1021/acs.langmuir.9b03578
*Langmuir* XXXX, XXX, XXX−XXX